CHALMERS
UNIVERSITY OF TECHNOLOGY

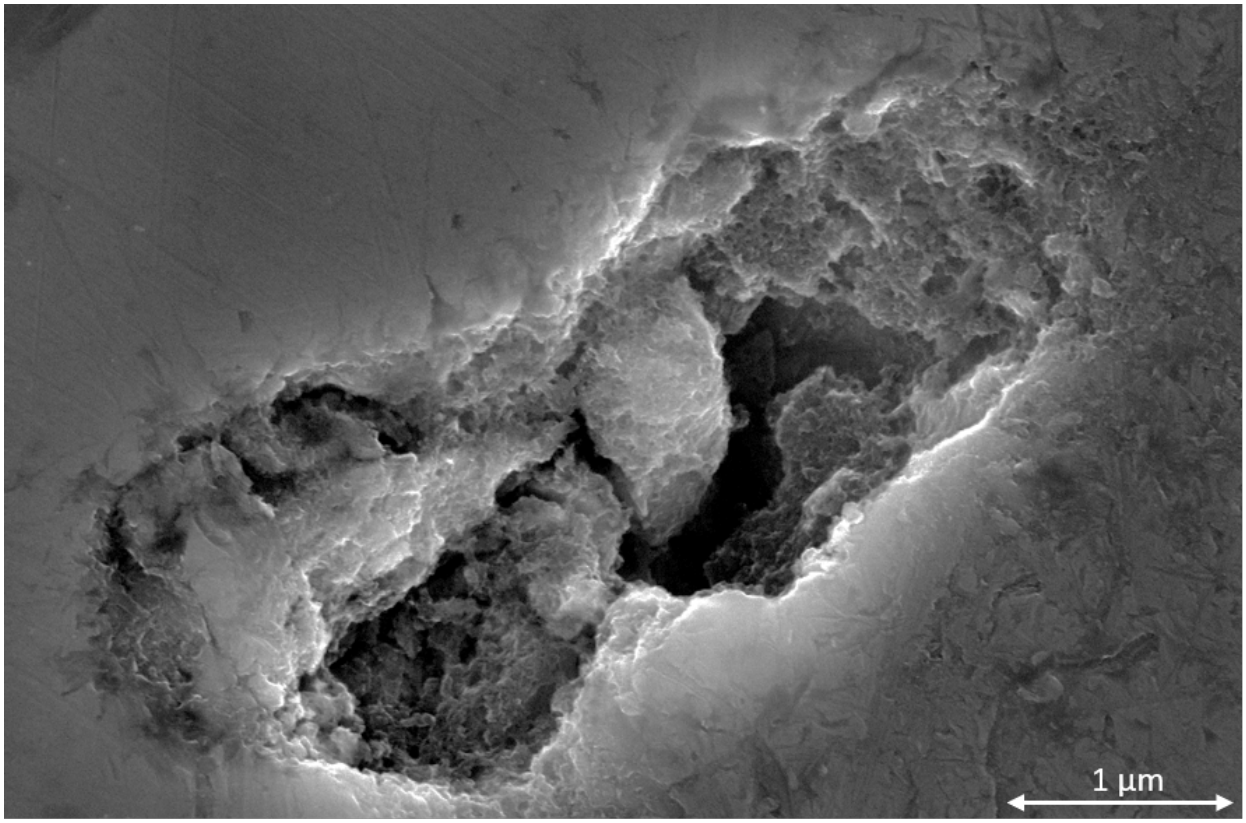

Porosity closure during hot isostatic pressing of additively manufactured Ni-based superalloy IN718 produced by LPBF and EBM

Argon porosity regrowth during subsequent heat treatment after HIP

Master's thesis work in Master materials engineering

Fredrik Liljestrand

Department of Industrial and Materials Science
CHALMERS UNIVERSITY OF TECHNOLOGY
Gothenburg, Sweden 2019

Master's thesis 2019

Porosity closure during hot isostatic pressing of additively manufactured Ni-based superalloy IN718 produced by LPBF and EBM

Argon porosity regrowth during subsequent heat treatment after HIP

Fredrik Liljestrand

CHALMERS
UNIVERSITY OF TECHNOLOGY

Department of Industrial and Materials Science
Division of Materials and Manufacture
Chalmers University of Technology
Gothenburg, Sweden 2019

Porosity closure during hot isostatic pressing of additively manufactured Ni-based superalloy IN718 produced by LPBF and EBM
Argon porosity regrowth during subsequent heat treatment after HIP
FREDRIK LILJESTRAND

© FREDRIK LILJESTRAND, 2019.

Supervisors: Dr Masoud Rashidi, Department of Industrial and Materials Science
Dr Anders Eklund, Quintus Technologies AB
Examiner: Prof. Eduard Hryha, Department of Industrial and Materials Science

Master's Thesis 2019
Department of Industrial and Materials Science
Division of Materials and Manufacture
Centre for Additive Manufacturing - Metal
Chalmers University of Technology
SE-412 96 Gothenburg
Telephone +46 31 772 1000

Cover: Scanning electron micrograph of a porosity in a specimen produced by laser powder bed fusion. This specimen was hot isostatic pressed at 150 MPa and 1120°C for 360 minutes.

Gothenburg, Sweden 2019

Porosity closure during hot isostatic pressing of additively manufactured Ni-based superalloy IN718 produced by LPBF and EBM.
Argon porosity regrowth during subsequent heat treatment.
Fredrik Liljestrand
Department of Industrial and Materials Science
Chalmers University of Technology

Abstract

Inconel 718 is a precipitation hardened Ni-based superalloy for aerospace applications where corrosion, creep and fatigue resistance are required. Additive manufacturing (AM) enables production of new designs of weight-optimised components with features not possible with traditional manufacturing techniques. However, components produced by additive manufacturing contain some defects such as gas porosity and lack of fusion defects (LOFD) which deteriorate the mechanical performance of the components. Hot Isostatic Pressing (HIP) utilises a high pressure up to 200 MPa in combination with a high temperature of up to 2000°C in a gas atmosphere to heal the defects in additively manufactured parts.
In this project, focus was placed on defect elimination in case of Inconel 718 components, produced by powder bed fusion technologies. To do so, two sets of cylinders (5 and 10 mm in diameter) were produced by laser powder bed fusion (LPBF) and electron beam melting (EBM). The cylinders contain a designed 1-mm sphere filled by un-molten powder in the centre of the sample. Pores contain processing gas, that is Ar in case of LPBF and gas residues from the vacuum in case of EBM. The specimens experienced 5 variants of HIPing cycles followed by 2 variants of heat treatments. All HIPing cycles were done at 150 MPa pressure and temperature of 1120 and 1180°C for duration between 5 and 360 minutes in 5 different combinations. Standard heat treatment for IN718 was performed inside HIP (pressurised heat treatment) or at atmospheric pressure. The LPBF and EBM specimens responded differently to the HIPing cycles. The HIPing cycles were not able to fully heal all gas porosities in LPBF specimens at applied conditions. Specimens from EBM were fully dense after HIPing for 1 hour. The LPBF specimens experience a re-growth of Ar porosity during atmospheric heat treatment compared to pressurised heat treatment in HIP. The microstructure inside the designed sphere is analysed in terms of oxide films, nitride inclusions, and prior powder boundaries.
The designed sphere filled by powders was seen as a relatively large lack of fusion defect, and this gave the possibility of following this defect during HIP and HT. The grain structure and precipitation of different phases are compared to the solidification microstructure achieved by laser and electron beam processes.

Keywords: AM, LPBF, EBM, HIP, IN718, Argon porosity, porosity reopen, regrowth

Acknowledgements

The work was performed in the framework of the Centre for Additive Manufacturing – Metal (CAM^2), supported by Vinnova. I would like to thank Quintus Technologies AB and especially Dr Anders Eklund for having the confidence to let me do this thesis work. In the department extra thanks will be given to Dr Masoud Rashidi and Professor Eduard Hryha, who have supported and guided me through this thesis. I would also like to thank my family and girlfriend for supporting me during the thesis time. Last but not least I would like to thank my friends who made the thesis a time full of joy and bearable in the stressful times. Thanks Bharat, Erica, Ismail and Kalol!

Fredrik Liljestrand, Gothenburg, June 2019

Contents

List of Figures

List of Tables

1
Introduction

Additive manufacturing (AM) entails all manufacturing techniques where a part is built from a 3D design by adding material layer by layer. AM enables unique possibilities both in terms of material composition and mechanical design [1],[2]. However, one of the drawbacks of AM is that the as built parts will often contain some defects, such as gas inclusions. This can be due to a number of reasons like bad process parameters, gas porosity in the powder or heavily reused powder. This results in defects such as lack of fusion defects (LOFD), gas entrapment during melting or oxide accumulations [3],[4].

LOFD usually have indication of the un-fused powder particles in the irregular pores or at one side of a crack-like defect in the printed part. Gas entrapment is another type of defect that gas appearance of a spherical pore and occurs when gas is trapped in the melt during solidification as well as gas trapped in the powder particles during the gas atomisation process [3],[5],[6],[7]. LOFD defects are also filled with the process gas. Hence, it is important to understand these defects, as they create stress concentrations which can adversely affect the fatigue life of a part.

One way to reduce the porosities is through hot isostatic pressing (HIP), which is typically motivated for components exposed to high mechanical and thermal cyclic stresses. This is especially useful in high performance parts that require optimised creep life, such as turbine blades. The HIPing process closes the porosities through plastic flow of the material and diffusion of the entrapped gas out of the component. However, some studies show that the pores reopen during subsequent heat treatments [3],[6],[8]. One hypothesis is that the atomic radius of argon is too big to allow for diffusion through the material, which results in the porosities not fully closing [3].

Inconel 718 is an alloy with excellent creep properties, hot corrosion resistance and oxidation resistance, and is therefore widely used in aerospace and turbines. It is an austenitic nickel-based age hardened material with γ'' as a main strengthener. The γ'' is a metastable precipitate and remains stable up to roughly 650°C [9],[10].

In this thesis, the impact of HIP on parts manufactured by LPBF in Argon atmosphere with respect to porosities closure and regrowth is investigated. The test samples are manufactured by laser powder bed fusion (LPBF) and Electron beam melting technique.

1.1 Scope

This thesis investigates the porosity closure of LPBF and EBM produced parts in the as-HIPped condition and after different heat treatments. The samples are designed to have a single large sphere in the middle of the specimen - the sphere is filled with unmolten powder.

In LPBF an argon atmosphere is used, therefore argon gas will be trapped in the sphere surrounding the unmolten powder. However, in EBM a vacuum is used, resulting in almost no gas entrapment within the sphere. The distance from the sphere to the outer surface of the part will be evaluated to determine if this distance affects the diffusion of the trapped gas. In other words, it will be evaluated if the distance of the sphere from the surface will affect the closure and reopening of porosity within the specimen. In the scope of this study, a closed sphere will be considered as a large lack of fusion defect. The effect on the microstructure of the defect boundaries will also be investigated.

Optimised process parameters were used and the samples were evaluated beforehand to ensure that no LOFD's were present. The microstructural changes during heat treatment and porosity caused by sub-optimal process parameters have not been explicitly examined in this thesis.

1.2 Aim

The aim of this thesis is to determine if Argon can diffuse through additive manufactured Inconel 718 during HIP by varying the HIP parameters and the cylinder thickness. By changing the thickness of the sample, the influence of a change in distance between the sphere and the surface can be evaluated. The intention is to determine if longer HIPing time will allow for better or full closure of porosities. The following research questions were investigated to answer these questions.

- Can Argon be eliminated during HIP of of Inconel 718?
- If the argon can not diffuse during HIP process, will pores regrow during subsequent heat treatment?
- If pores do not fully close and reopen during ageing, can ageing inside the HIP under high pressure increase the toughness of the material?
- Does the distance of the porosity to the surface affect the reopening of the porosity after heat treatment?
- How will the microstructure look in a HIPped LOFD in Inconel 718?

2
Theory

In the following chapter, the fundamental principles of the used techniques will be described.

2.1 Additive manufacturing

Conventional machining is subtractive in nature, in that material is removed from the bulk material in order to form a part. Additive manufacturing (AM) differs from this as it starts from a 3D file that is compiled by computer aided design (CAD). The file is then sliced mathematically into 2D layers [1].

In powder bed fusion AM, powder is spread as an evenly distributed thin layer which is then melted together with the previous layer of the part according to the CAD file [1],[2]. In this way, the part is built additively layer by layer.

AM has many benefits over traditional manufacturing. For example, new complex designs like internal cooling channels that was not possible to manufacture before, can now be intrinsically added to the design. The part is built to be near net shape and little post processing is needed [2]. The powder for AM is very fine and should be formed spherical to have a good flowability. The powder should also have a good spread in size to maximise the packing density [11].

In this thesis two different techniques of AM is used. Both of these techniques are powder bed fusion techniques where a thin, evenly distributed layer of powder is fused together by a power source. The manufacturing has to take place in a protective environment that could be a noble gas or vacuum. The powder is spread by a powder spreader/ recoater blade. This blade can be both a hard metallic blade or a soft blade. The power source then melt the contour of the part then finishing the layer by melting the bulk of the material with hatches. Next powder layer is applied and the process is repeated. [1],[2].

2.1.1 Laser powder bed fusion, LPBF

LPBF is the most widely used AM process because of its versatility. A schematic of LPBF process can be seen in figure 2.1. The material is melted/ fused by a laser that is moved by mirrors. The chamber is subjected to slight over pressure conditions with an inert gas like Ar or N_2 [2]. The layer thickness is around $20-50\,\mu m$ [11].

The focus of the laser is finer than EBM and smaller particles are used which gives the build a lower surface roughness [12].

The printed part require supports to transport the heat away, and to withstand thermal stresses and forces imposed by the powder spreader. These supports allow for heat dissipation away from the part - in other words, heat is removed from the part, down into the build plate. Supports in AM are included in the CAD design and printed as part of the build process. The supports should be designed in such a way that they are easy to remove after the build is completed [13].

The high cooling rate of the melt is sometimes desirable, but is possible to lower by heating the building plate in case of brittle materials. This can be a problem with some brittle materials that could crack during solidification. The success of the build and its defects mostly depend on process parameters such as scan speed, laser power, hatch distance, hatch overlay. The parameters control the microstructure and thereby the mechanical performance. After the build, the part needs post processing to relieve residual stresses [2].

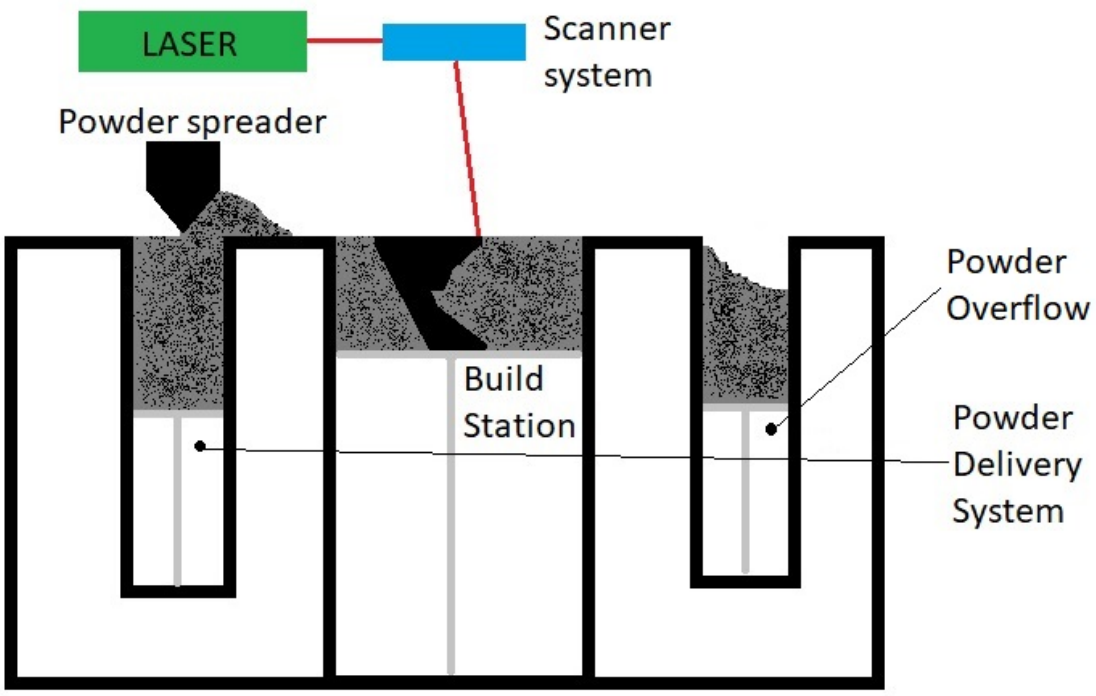

Figure 2.1: Schematic of LPBF machine

2.1.2 Electron beam melting, EBM

EBM is not currently as common in industry as LPBF - however, there are several similarities between the processes. The main difference is the power source - for EBM, an electron beam is used instead of a laser to fuse the powder. The electron beam is moved with electromagnetic lenses, which are much faster than a physical

mirror. To avoid deflection of the electron beam by gas molecules the chamber is kept under vacuum [12].

The powder needs to be slightly bigger than that used for LPBF. This is because the powder particles get charged by the electron beam and thus do not repel each other easily. The spot size is more diffused and larger for EBM as compared to LPBF [14]. The increased power allows EBM to have a thicker layers and larger powder particles and therefore increases productivity. Each powder layer is pre-sintered by the electron beam before melting starts, which lowers the thermal gradient in the part. This in turn reduces the stresses in the part. It is therefore possible to use EBM to manufacture parts from more brittle materials, like titanium almuminide [14].

During heating, a light sintering of the powder takes place in order to prevent the powder particles from flying away due to the charge from the electron beam. The part can be built at a higher temperature that allows the part to be annealed during the build and minimises the need for post processing [12],[14].

As in LPBF, the defects mostly depend on the process parameters. However, a larger number of process parameters plays a role during EBM, including beam power, beam diameter, beam scanning velocity and beam line spacing [2].

2.1.3 Defects in AM

There are different defects commonly seen in AM, these defects are lack of fusion defect (LOFD), gas porosity and shrinkage porosity.

Lack of fusion defects are created from insufficient melting. The insufficient melting often arises when the volumetric energy input from the power source is too low. The defect is often irregular in shape and has unmolten powder particles. In EBM the LOFD are often seen in the interface between the hatch and contour region [4]. The porosity will be filled with the gas or vacuum from the building chamber.

Gas porosities have a spherical shape and often containing gas from the powder manufacturing or entrapped during melting process. During the powder manufacturing through gas atomisation, gas can be trapped as small near-spherical porosities inside the powder particle. The porosity is then trapped inside the solidifying layer during manufacturing and do not have sufficient time to escape the melt. These porosities can thereby contain gas even in EBM samples that are produced in vacuum [6].

Shrinkage porosity can sometimes be seen throughout the sample. These are formed in the interdendritic regions during the rapid cooling during solidification. When the dendrites have solidified and shrink because of the thermal expansion there is an incomplete flow of melt to the desired regions, resulting in fine porosity [15].

2.2 Hot isostatic pressing, HIP

Porosities arise from solidification cracks, gas entrapment or lack of fusion defects during AM manufacturing techniques. On way to remove these porosities are hot isostatic pressing (HIP). HIP utilises high pressure and high temperature to collapse these pores. The pores can then heal by diffusion and become fully closed. The basic driving force for densification is to decrease the surface area of the pores. The fundamental reason for doing HIP is to remove porosity defects in manufactured parts [8].

Pores are enclosed by a high isostatic pressure at a high temperature. In essence, the part is subjected to an isostatic pressure on all open surfaces by an inert gas. The high temperature allows the material to flow plastically and close the pores. After enough time the pore surfaces bond together by diffusion and fully close the porosity [8]. If the temperature would be too high, unacceptable grain growth will occur. The three parameters are time, temperature and pressure. By increasing the pressure, temperature can be lowered and unacceptable grain growth can be avoided [8].

As the pores are shrinking, the gas pressure inside the pore will increase. The gas needs to diffuse away to a volume with lower energy, i.e. the outer surface. Normal paths for diffusion or vapour transport includes grain boundaries, lattice or surface paths [8]. If the gas cannot diffuse via one of these diffusion paths, or if there is not sufficient time to diffuse away, it will form an equilibrium size dependent on the applied pressure. During subsequent heat treatment at atmospheric pressure, the pores will then regrow and form a new equilibrium size [8].

2.3 Inconel 718

Inconel 718 is an austenitic nickel-based superalloy that has a working temperature of up to 650°C. Its main strengthener is the disc shaped metastable γ'', although it is also strengthened by the spherical shaped γ'. The γ'' has a body centered tetragonal (BCT) structure and consists of Ni_3Nb. It works as a coherent precipitation strengthener in the γ matrix, creating high mismatch strains of up to 2,9% [18]. γ'' forms intragranular during ageing.

If aged too long, the γ'' transforms into the stable δ precipitate. The δ also consists of Ni_3Nb, but forms larger incoherent precipitates - this is undesirable in the matrix due to its negligible hardening effect. However, some needle shaped δ precipitates at the grain boundaries are beneficial, as it prohibits grain boundary sliding which improves ductility in rupture tests [16],[17].

The γ' phase forms during ageing - this has a face centered cubic (FCC) structure that consists of Ni_3(Ti,Al) [18]. The laves-phase is an undesirable phase as it is a brittle, intermetallic phase containing high amounts of Nb, Mo and C. This usually

forms in the interdendritic region due to segregation of the solute. In conventionally manufactured Inconel 718, long homogenisation heat treatments is used to dissolve the laves-phase [7], [19]. In AM, increased beam power results in a lower thermal gradient, resulting in a higher amount of laves-phase [19].

The main carbide former in IN718 is Nb; however, it can also contain Ti. During solidification, these MC-type carbides are formed mainly in the interdendritic areas that are rich in solute. They nucleate and grow on Ti nitrides that have solidified at a higher temperature in the melt [24]. Because of the high solution temperature (1250°C) of these MC carbides, it is not possible to remove them through heat treatment [20],[7]. Although MC carbides are not the only type of carbides in IN718, it is the most common. Other types of carbides found in IN718 are M_6C and $M_{23}C_6$. These carbides are found in cast and wrought IN718 [22],[21]. However, it is uncommon in AM IN718 and currently there is no relevant literature available on this. M_6C is a complex carbide consisting of Mo, Cr, and/or Nb and is not formed if the Si-content is below 0,1%. It is formed during high temperature exposure from super saturated solution in the temperature range of 816-982°C [21],[18]. $M_{23}C_6$ can form during high temperature exposure between 790-816°C - although it can form at higher temperatures up to 920°C. It is an undesirable complex carbide that can vary significantly in composition, and it typically forms carbide films at the grain boundaries [18],[22]. Table 2.1 shows a summary of the different IN718 phases [10],[23],[24].

Table 2.1: Phases in IN718

Phase	**Crystal structure**	**Chemical formula**	**Solvus temp,°C**
γ	FCC	Ni	1340
γ''	BCT	$Ni_3(Nb)$	900
γ'	FCC	$Ni_3(Ti,Al)$	750-910
δ	orthorhombic	$Ni_3(Nb)$	1025
MN	Cubic	(Ti,Nb)N	1450
MC	FCC	(Nb,Ti)C	1250
M_6C	FCC	$(Mo,Cr,Nb)_6C$	982
$M_{23}C_6$	FCC	$(Mo,Cr,Nb)_23C_6$	816
Laves	HCP	$(Ni,Fe,Cr)_2(Nb,Mo,Ti)$	1150

2.4 Heat treatment

It is typically recommended that the first post heat treatment is applied while the parts are still attached to the build plate - this is to allow for relieving of residual stresses in the IN718 parts produced through LPBF [25]. For traditional cast and forged materials, homogenisation solution heat treatment is employed to dissolve the laves-phase and δ phase - the same process is applied for parts produced by AM. Different ageing procedures can be used to ensure that the material is homogenised, depending on the intended application of the part. The purpose of ageing is to

precipitate the strengthening phases γ'' and γ'. Standard heat treatment procedures for wrought and cast materials in accordance to AMS 5664 is provided in table 2.2, [26].

Table 2.2: Heat treatment according to AMS 5664 [26]

Heat treatment	**Temperature, °C**	**Time, h**
Solution	1065	1-2
Age 1	760	10
Age 2	649	8-10

2.5 Powder manufacturing

Powder for AM has special requirements, specifically to ensure the spherical shape and a good size distribution. There are several techniques currently used to manufacture powder for AM.

2.5.1 Gas atomisation

The most common process currently is inert gas atomisation - a schematic of the process can be seen in figure 2.2. The process starts with induction melting of the feedstock material. The molten material is fed through the atomisation nozzle where the melt is directed by a high flow of inert gas - usually argon or nitrogen. This breaks up the melt into small droplets that solidify at a rate between 10^3 to 10^6K/s, depending on particle size, media and process conditions. The droplets fall to the bottom of the chamber and further sieved to the desired particle size. The finest powder travel with the inert gas stream to the gas pump and is collected in the second chamber [27].

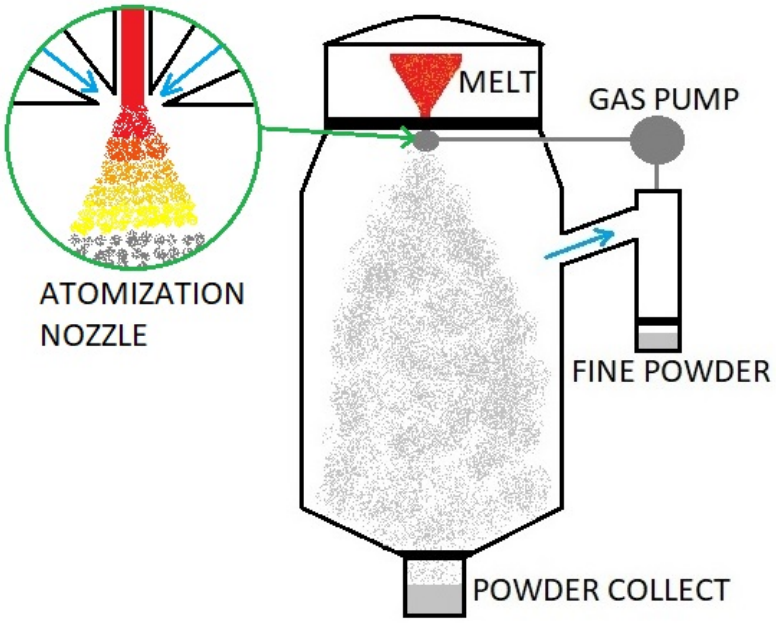

Figure 2.2: Schematic of gas atomisation, blue arrow indicates gas flow direction

2.5.2 Plasma atomisation

Plasma atomisation is very similar to gas atomisation, with the main differences being the type of feed stock and the melting method. In this case, the feed stock is a wire which is melted using high velocity plasma instead of induction melting. The plasma gas is usually argon. This process results in minimised contamination, as the molten material does not come into contact with any solid surface before solidification. The temperature of the plasma is higher than in conductive melting - this results in longer solidification time of the droplets, thus ensuring a spherical powder with high purity. This process is more expensive but results in a powder with the desired shape and equal purity compared too powder obtained through gas atomisation [28].

3
Methods

This chapter provides an overview of the methods used during this thesis.

3.1 Literature study

Search engines including Google, Google scholar and the discovery service for Chalmers University of Technology has been used for this literature study and relevant articles have been cited.

3.2 Design of experiments

To answer the research questions posed in this thesis, samples as shown in figure 3.1, were manufactured. Four series of cylinders with spheres were manufactured by both LPBF and EBM processes. The samples were then tested under different HIPing and ageing conditions. Cylinders with two different diameters were produced to understand the influence of the distance between the pore edge and the surface on porosity removal.

The sphere in the middle of each cylinder is small (1 mm in diameter) - it could therefore easily be missed during grinding. To make it as easy as possible to locate the sphere, the samples were designed with a two step marking. The first step indicates the edge of the sphere, whilst the second marking indicates the middle of the sphere. To simplify mounting, a flat surface was added parallel to the marking steps, as shown in figure 3.1.

Each cylinder was evaluated to determine the amount of porosity present inside the sphere. The original intent was to use these results in order to determine the optimal HIPing and heat treatment parameters for toughness testing samples. Due to time constraints of the project, it was decided to HIP and heat treat these toughness testing samples at the same time as the cylinders used for the porosity evaluation. Therefore, there is less samples on HIP 5 compared to the rest of the cycles. The number of impact bars that underwent different heat treatment cycles is detailed in table 3.2.

Figure 3.2 shows the impact testing bar with the sphere inside. The small triangles on the top indicates where the notch should be placed. The notch was planned to be milled down after machining using a standardised notch tool. The samples were

Table 3.1: Samples manufactured by LPBF and EBM consisted of two series each of 5 mm and 10 mm cylinders. In total 96 small cylinders were produced and tested. The second column named "with marking" is samples for light optical microscope images evaluation from a cross section. The third column named "No marking" is fully cylindrical samples meant for planned CT scanning.

Heat treatment	**With marking**	**No marking**
As built	2	1
HIP 1, No Age	2	1
HIP 1, atmospheric ageing	2	1
HIP 1, Pressurised ageing	2	1
HIP 2, No Age	2	1
HIP 2, atmospheric ageing	2	1
HIP 2, Pressurised ageing	2	1
HIP 3, No Age	2	1
HIP 3, atmospheric ageing	2	1
HIP 3, Pressurised ageing	2	1
HIP 4, No Age	2	1
HIP 4, atmospheric ageing	2	1
HIP 4, Pressurised ageing	2	1
HIP 5, No Age	2	1
HIP 5, atmospheric ageing	2	1
HIP 5, Pressurised ageing	2	1

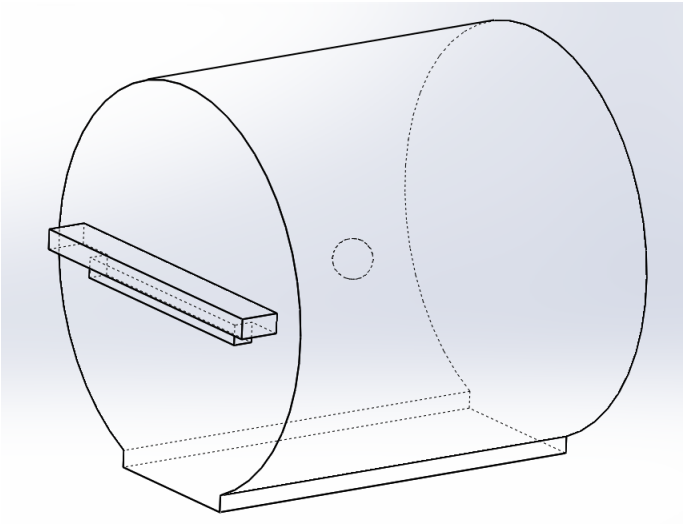

Figure 3.1: Markings showing porosity in cylinders and also the flat surface to level the markings.

printed slightly bigger so they could be machined down to the correct size according to ISO 148 - the standard size is 10mm x 10 mm x 55 mm, while the printed size was 11mm x 11mm x 57mm. Due to time constraints for this project, the impact toughness samples will be tested and evaluated in a follow-up project.

Table 3.2: Impact bars manufactured by LPBF. Samples named "Por, Sphere" are samples with the built-in sphere with unmolten powder. Samples named "Solid" are solid samples for reference. A maximum of 120 impact bars could be fitted on the build plates during printing. When the HIPing cycle started, it was determined that the following samples mentioned in this table would be evaluated.

	X/Y direction		**Z direction**	
Heat treatment	**Por, sphere**	**Solid**	**Por, sphere**	**Solid**
As built	1	1	1	1
Heat treated, Ageing, No HIP	2	2	2	2
HIP 1, No Age	1	1	1	1
HIP 1, Atmospheric ageing	1	1	1	1
HIP 1, Pressurised ageing	3	3	3	3
HIP 2, No Age	3	3	3	3
HIP 2, Atmospheric ageing	3	3	3	3
HIP 2, Pressurised ageing	3	3	3	3
HIP 4, No Age	3	3	3	3
HIP 4, Atmospheric ageing	3	3	3	3
HIP 4, Pressurised ageing	3	3	3	3
HIP 5, No Age	1	1	1	1
HIP 5, Atmospheric ageing	2	2	2	2
HIP 5, Pressurised ageing	1	1	1	1

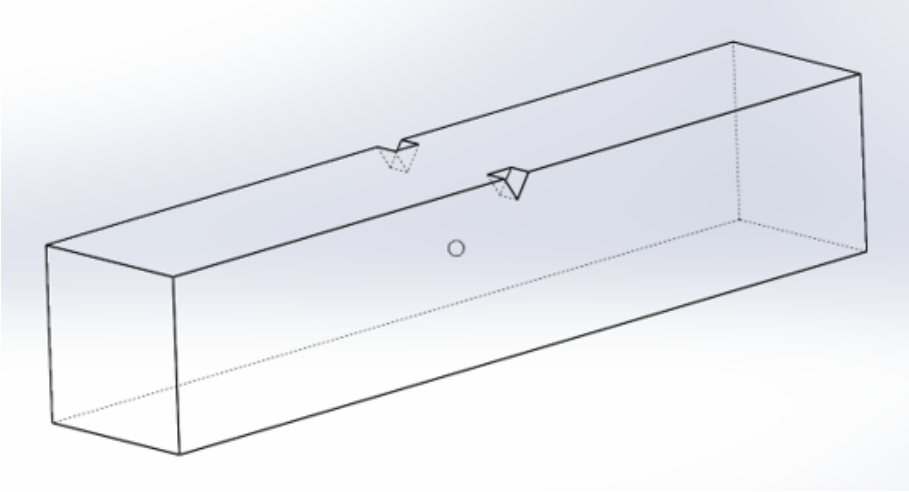

Figure 3.2: Impact toughness test bar. The small triangles show where the sphere is located in the bar so that after machining the notch can be placed at the correct position.

3.3 LPBF manufacturing

The LPBF samples were manufactured using an EOS M290 machine at Chalmers. This machine uses a 400 Watt Yb-laser and has a build platform of 250mm x 250mm x 325 mm. 3Standard process parameters for In718, provided by EOS, were used in this study. The powder had a size distribution between 20 and 53 µm and was

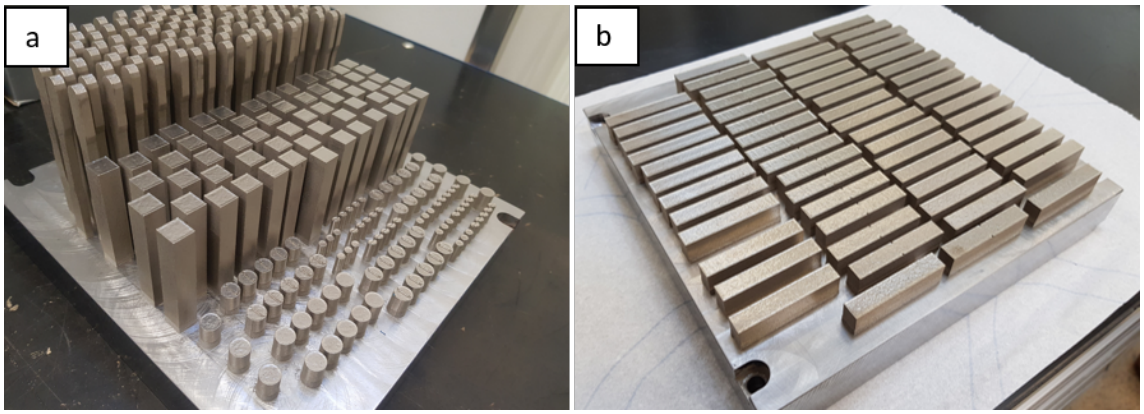

Figure 3.3: All produced samples by LPBF before they were removed from the build plates. a, build plate 1. b, build plate 2.

supplied by Höganäs. Chemical composition of this powder is given in table 3.3. Powder has been reused several times, resulting in a small amount of accumulated oxides on the surface. The build plates can be seen in figure 3.3 where figure 3.3(a) shows the X/Y direction impact bars and cylinders. In figure 3.3(b), the Z direction impact bars are shown.

Table 3.3: Inconel 718 powder

Material	Ni	Cr	Mo	Nb	Ti	Al	Si	C	Fe
Wt, %	52	18,5	3	5,2	0,9	0,7	0,4	Max 0,04	Balance

3.4 Metallographic preparation

The samples were mounted with Struers PolyFast (conductive resin) and ground down with grit 120 at minute-long intervals until the first sign of the porosity or the porosity marking. This was followed by finer grit sizes - 220, 500, 800, 1200 and last 2000. The samples were then polished with diamond suspension from Struers DiaPro in three steps: Allergo/Largo 9 µm, then Dac 3 µm and finally Nap B 1 µm. To see the microstructure in the as-built and as-HIPed samples, they were electrolytically etched with oxcalic acid applying a voltage of 3,5 V. For samples that were aged, Kalling's no. 2 reagent was used to electrolytically etch with a voltage of 3.5 V.

3.5 Porosity measurement

The usual porosity in the material resulting from the building processes were identified by using pictures taken with the light optical microscope. The pictures were then evaluated with the open source program ImageJ. The first step in the image processing entails removal of the scale-bar - if this is not done, an increased amount

of porosity would be shown. The colours were then changed to black and white 32-bit and a threshold adjustment was performed. This threshold adjustment ensures that only the black areas are shown. Unfortunately, there is no way to differentiate between oxides and porosities. Examples of a threshold adjustment with identified porosities can be seen in Appendices A.1 and A.2.

3.6 SEM

High resolution micrographs were taken with the Zeiss-LEO 1550 field emission SEM at Chalmers University. An "In-lens" secondary electron detector was used for topographic images. However, topographic images with compositional contrast was made with a "Centaurus" back-scattered detector (BSE). An electron dispersive X-ray (EDX) detector was used for the chemical analysis.

3.7 Hot isostatic pressing

The HIP was done by Quintus technologies in Västerås, Sweden. The machine used was a QIH21, which is a compact machine intended for small scale production and research. The furnace inside this machine is a Uniform Rapid Cooling (URC) type furnace with a cooling rate of up to 200°K/min. The furnace has a cylindrical work area of 228 mm x 700 mm. The applied HIP cycles are given in table 4.1 and visually represented in figure 4.1.

3.8 Heat treatment

Inconel 718 is a precipitation hardened alloy. To develop these precipitates in the matrix, the material undergoes a two step ageing heat treatment. The first ageing cycle in this study was done inside the HIP furnace under pressure. The second ageing cycle was the standard ageing cycle for rotational parts as a reference. These ageing cycles can be seen in figure 3.4.

In this study, ageing inside the HIP furnace will be referred to as pressurised ageing. The standard reference ageing is done according to AMS 5664 as detailed in table 2.2 [26]. For the standard ageing, a two hour solution treatment cycle was performed before the ageing cycle started. The pressurised ageing did not go through a solution treatment cycle before ageing. The samples aged inside the HIP furnace is cooled at a much higher rate compared to the furnace cooled standard ageing cycle - this is made possible through the use of the URC furnace.

The pressurised ageing is performed at a pressure of approximately 100 MPa - this is lower than the pressure used in the HIPing cycles. When the temperature is decreasing after the HIP, the pressure also decreases with the temperature according to the ideal gas law. The 100 MPa at 760°C is an equivalent pressure to 150 MPa at 1120°C.

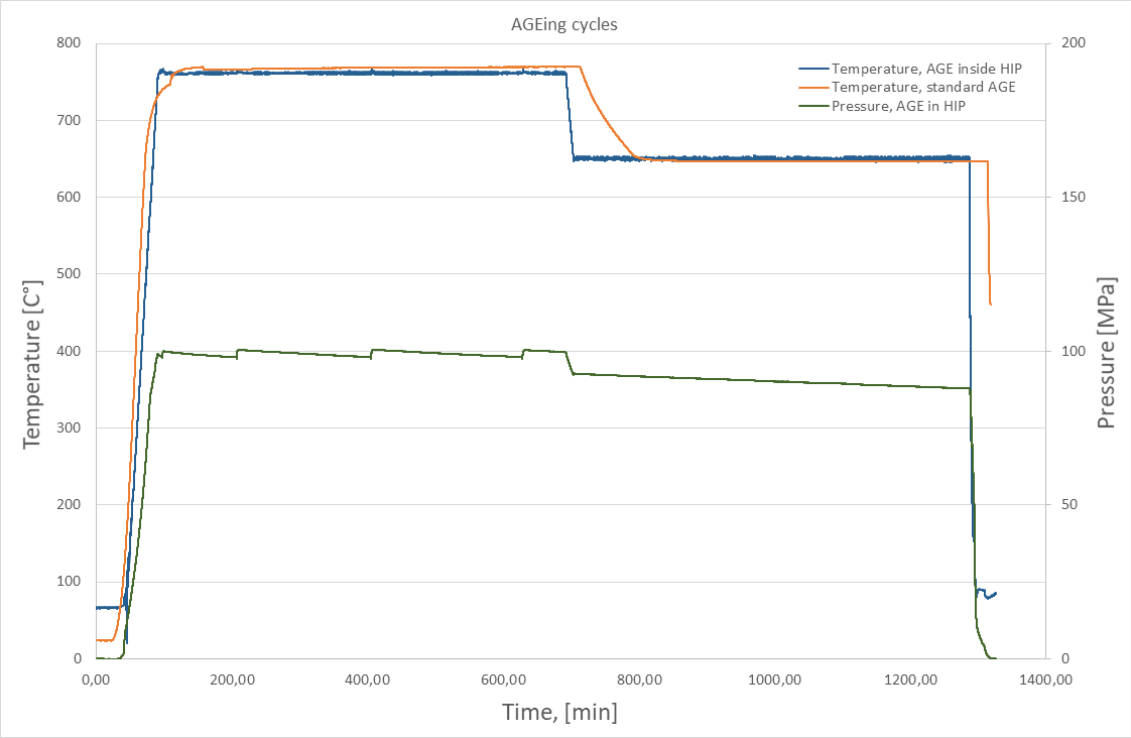

Figure 3.4: Ageing cycles

4

Results & Discussion

4.1 HIP parameters

The holding times and temperatures of the different HIPped samples are given in table 4.1 and represented in figure 4.1. In the HIP 1 cycle, the intent was only to reach 1120°C, then finish the cycle. However, a hold time of 5 minutes was kept to ensure that the parts had enough time to reach the target temperature. This temperature (1120°C) was chosen to avoid abnormal grain growth in EBM produced samples [29].

During evaluation of porosity closure in the HIP 4 cycle (1120°C, 6 hours, 150 MPa), it was apparent that the porosity was not fully closed. To confirm that the temperature was not too low, another set of samples were produced - this resulted in the HIP cycle 5 sample set, which was HIPped at an increased temperature of 1180°C.

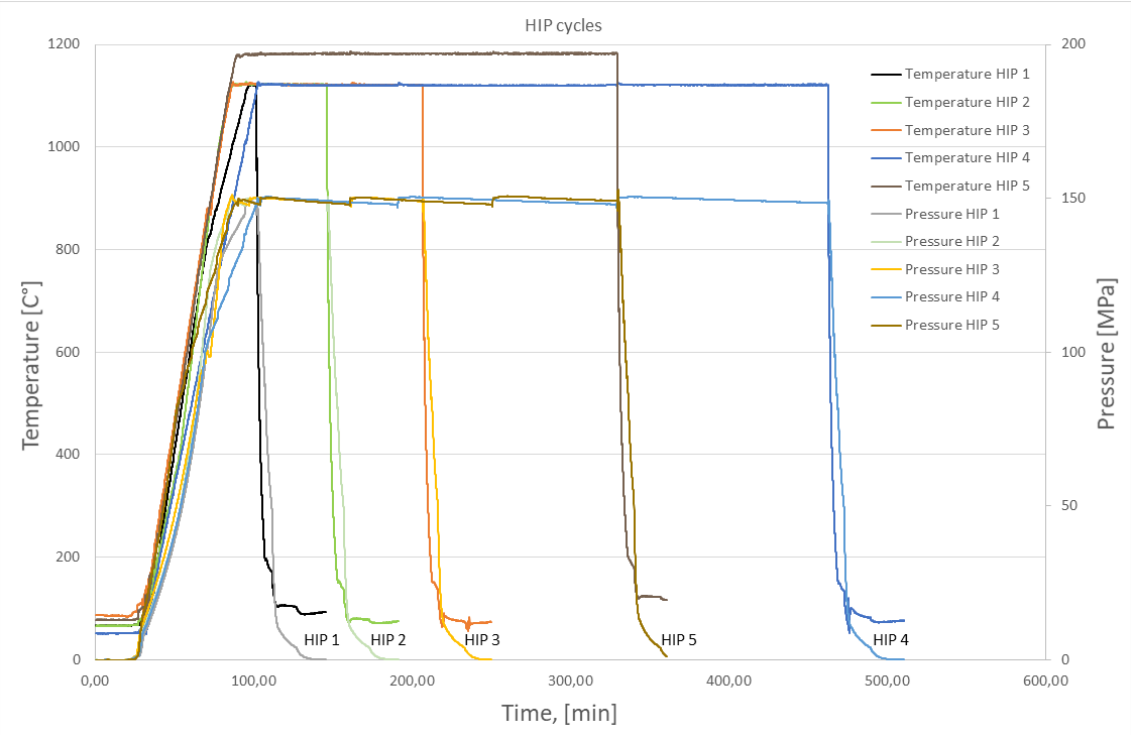

Figure 4.1: HIPing parameters. The Y-axis on the left show the temperature and the Y-axis on the right show the pressure. The X-axis show time in minutes.

Table 4.1: HIPing parameters. All used HIPing cycles and their parameters are shown.

Name	**HIP 1**	**HIP 2**	**HIP 3**	**HIP 4**	**HIP 5**
Temperature, °C	1120	1120	1120	1120	1180
Pressure, MPa	150	150	150	150	150
Time, min	5	60	120	360	240

4.2 Printed void, as built

The sphere in the middle of the sample was designed in CAD. Cross sections of some of the as built spheres can be seen in figures 4.2 and 4.3. During the printing process, only the powder along the contour of the sphere was melted at each layer. In the bottom of the sphere, the heat from the laser or electron beam could be conducted away. This resulted in a rounder shape in the bottom of the sphere as compared to the top. On the upper part of the sphere, the beam would melt deeper because there is no solid material underneath which could conduct the heat away. This resulted in a flatter top with more partially-fused powder particles adhering to the molten surface.

4.2.1 LPBF

The sphere has a fine resolution because of the fine powder size distribution, small layer thickness (40µm) and narrow spot size. This results in the sphere having an almost round bottom with only a few fused powder particles adhering to the sphere. The top of the part has a large overhang which means there will be more partially-fused powder particles adhering to the sphere. In figure 4.2(a), the expected round bottom and flat top can be seen - it can also be observed that the flat top has more attached powder particles than the bottom. As can be seen in figure 4.2(b), the laser has melted deep into the powder of the sphere. During sample preparation of the as built samples, the powder inside the sphere would fall out. Therefore, the sphere seems to be empty with only a small amount of adhered powder particles on the inside of the sphere.

4.2.2 EBM

The coarser particle size distribution, layer thickness and spot size in EBM gives the sphere a step-like surface. The bottom of the sphere is almost flat, most probably because it is the top of a molten layer. In figure 4.3(a), there are still many lightly-fused particles covering the inside of the sphere - these powder particles have not fallen out during grinding or polishing. In figure 4.3(b), the build layers can be seen as well as the bottom of the sphere, with only a few adhered partially-fused powder particles visible. On the top, partially-fused powder particles adhere to the upper part of the sphere as expected.

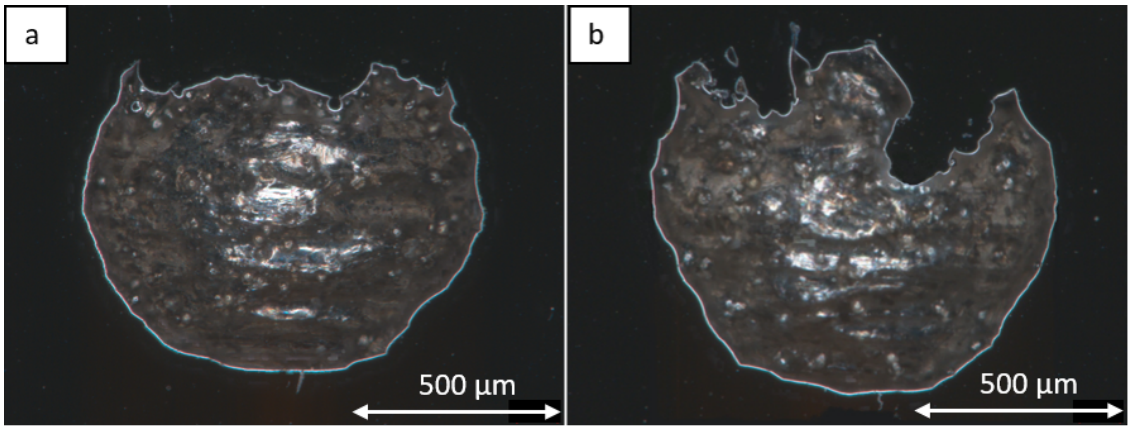

Figure 4.2: LPBF, as built cylinders showing printed sphere. a, 5 mm cylinder, b, 10 mm cylinder.

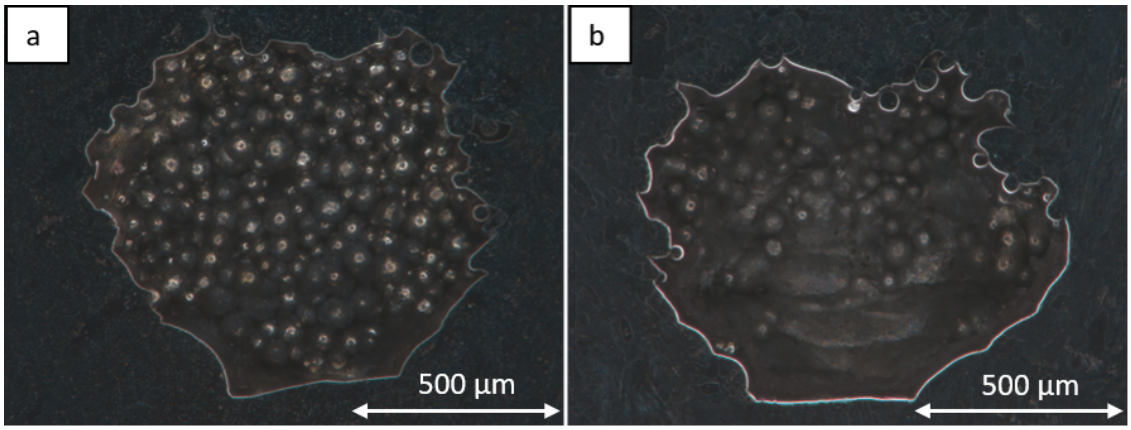

Figure 4.3: EBM, as built cylinders showing printed sphere. a, 5 mm cylinder, b, 10 mm cylinder.

4.2.3 LPBF vs EBM

Samples produced by both LPBF and EBM have pore of the size as required. However, samples produced by LPBF have better spherical shape than the EBM because of the higher resolution of the process [2].

4.3 Porosity

The average porosity in the material surrounding the sphere in the center of the sample is a result of the AM process. The sphere is excluded from these results, as seen in figure 4.4, and the referred HIP cycles are shown in figure 4.1. These values are calculated from the light optical microscope images. The porosity content evaluation is complicated because of the dark colour of inclusions, oxides and carbides, which therefore resembles small gas porosities. They therefore increase the average porosity count even doe the porosity do not increase. MC type carbides are shown to grow and nucleate at grain boundaries during longer HIPing cycles [30], [31]. These

carbides increase the overall amount of porosity count at HIPing times longer than 2 hours. In this study, HIP Cycles 4 and 5 are long enough to see carbide growth - this can be seen in figure 4.4.

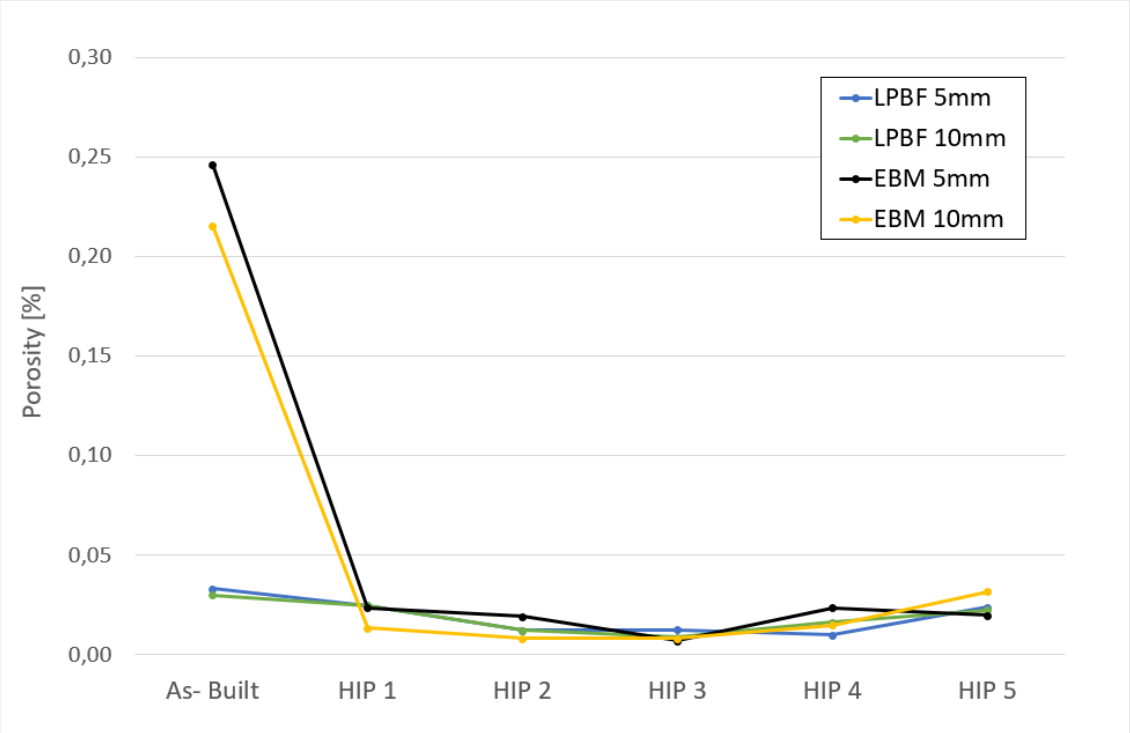

Figure 4.4: Average porosity after each HIP cycle

4.3.1 LPBF

The LPBF samples in as built condition contained mainly two types of defects: gas porosities and some oxide inclusions. An example of gas porosity from an EBM sample is shown in figure 4.5(c). No LOFD were found in the LPBF manufactured samples, which indicates good process parameters.

4.3.2 EBM

The defects found in as built EBM samples were mainly shrinkage porosities and gas porosities; however, a few LOFD were also found. In figure 4.5 examples of these defects are shown. The shrinkage defects are mainly located in the region of the interface between hatches and between contour and hatch [29].

4.4 Microstructure

The microstructure outside the sphere contains elongated grains in the building direction because of the heat flux direction. In the light optical microscope (LOM)

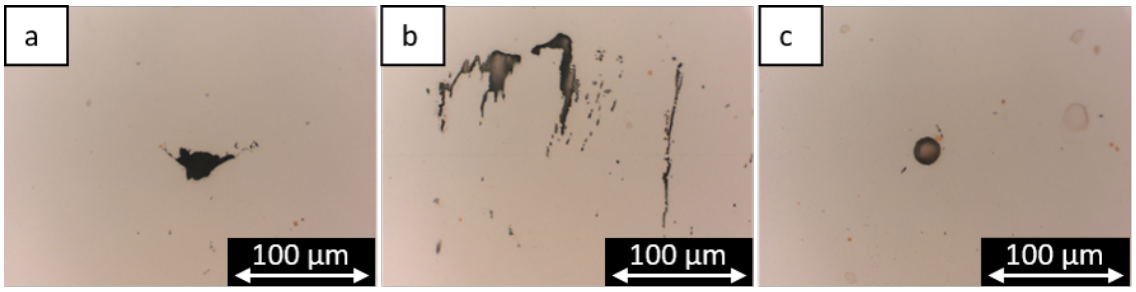

Figure 4.5: As built EBM 10 mm cylinder. a, Lack of fusion defect. b, Larger LOF porosity. c, gas porosity.

only oxides, carbides and nitrides are visible. After etching the grain boundaries are also visible.

Many carbides and nitrides were visible in the light optical microscope images. The SEM with EDX detector was used to confirm that the yellow areas are titanium nitrides growing on aluminium oxides - see figure 4.6. This is also supported by literature [20],[23],[24],[32]. These aluminium oxides often have yellow nitrides next to them. These nitrides will in turn act as nucleation sites for MC-type carbides, which solidify shortly before the γ-matrix at 1350°C. They are therefore often seen together [20],[23],[24].
These nitrides were much larger in size in the LPBF than in EBM, which indicates that the LPBF powder is gas atomised using nitrogen gas. The fact that these nitrides originates from the powder is further confirmed as they do not dissolve during melting with the laser [20],[23],[24],[4]. The larger size of the nitrides would in turn increase the nitride content in the sample. The EBM powder inside the porosity contains larger Nb carbides compared to the LPBF powder. These carbides have a light grey colour in the light optical microscope and are easy to distinguish from the titanium nitrides - this is shown in figure 4.7. These variations in carbide and nitride contents are due to the different powder manufacturing techniques as well as process conditions during AM processing. During EBM processing AM component is held at a temperature around 1000°C for dozen of hours, resulting in the carbide precipitation, not seen in LPBF process due to the rapid cooling.

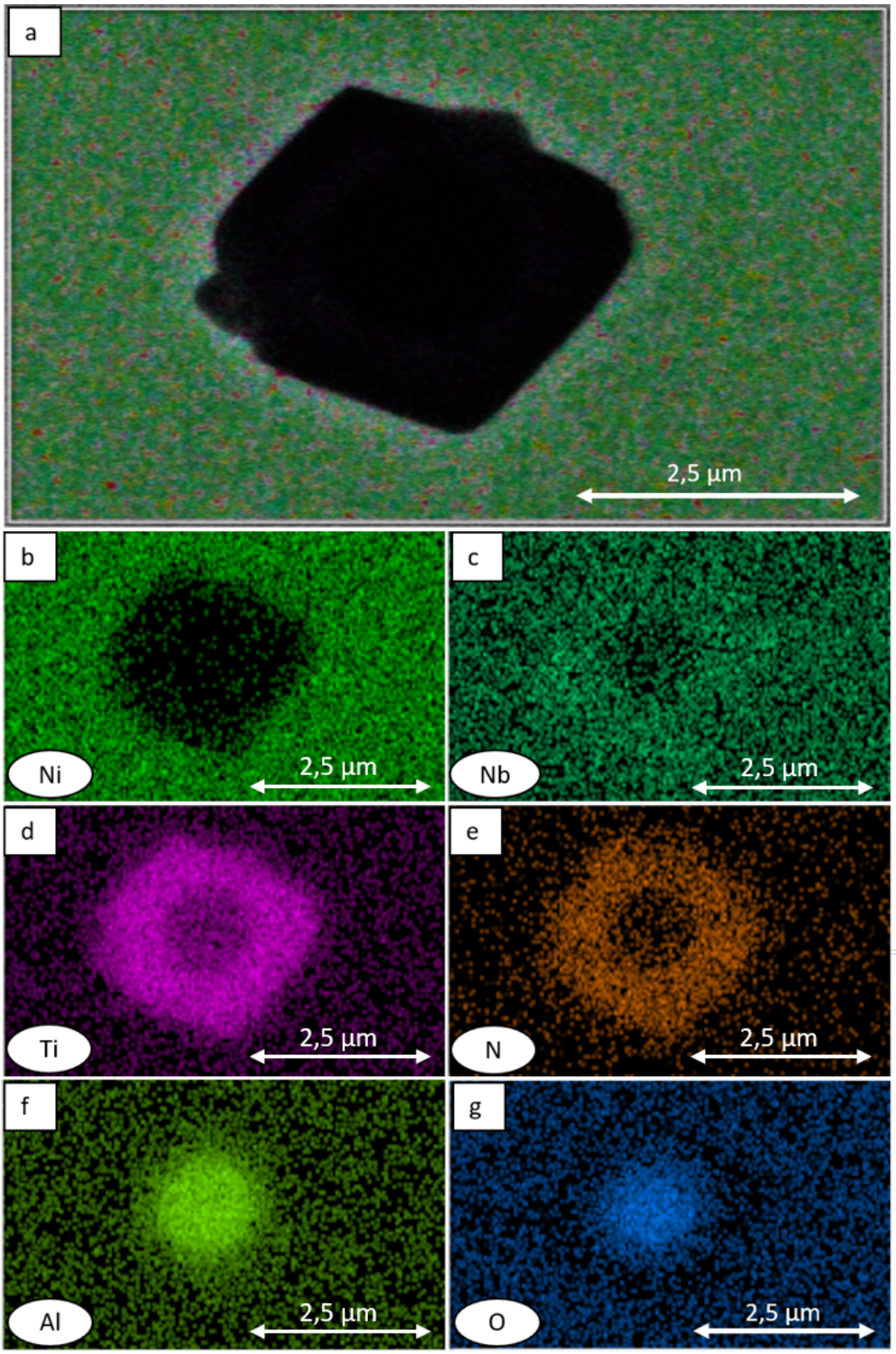

Figure 4.6: EBM, HIP 3, as HIPped, 5 mm cylinder. a, mapped area of nitride growing on an oxide. b-g, composition of nitride and oxide.

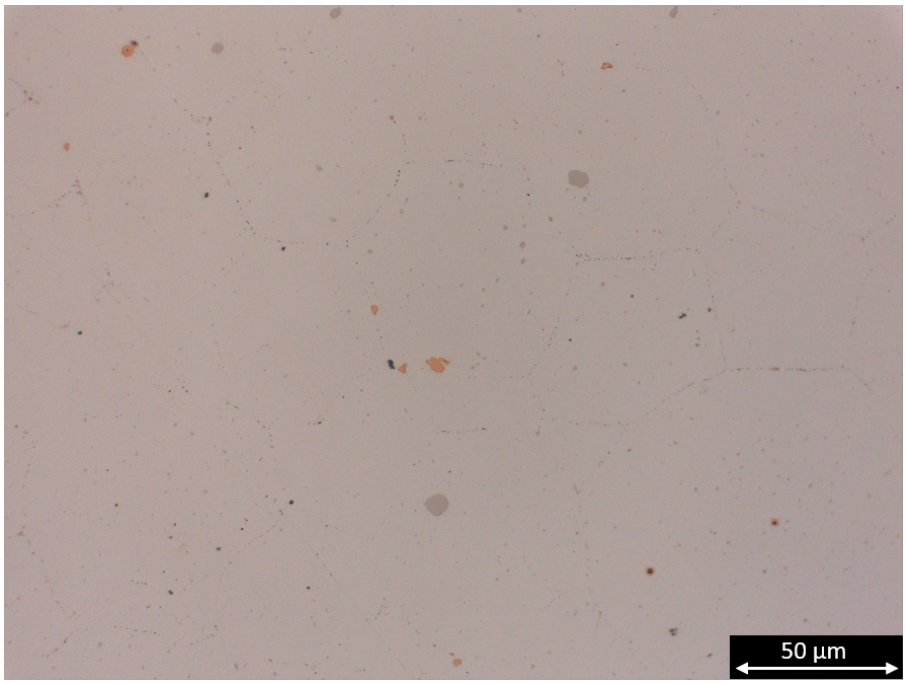

Figure 4.7: EBM, HIP 5, standard ageing, 5 mm cylinder, inside sphere, this figure shows both large niobium carbides that are grey and titanium nitrides that are yellow. Previous particle boundaries are also visible.

4.5 Void closure after HIP

In the cross section of each of the samples (both from LPBF and EBM), an oxide layer was present at the bottom of the built sphere. The oxide layer is thicker and cover larger area in the samples built in LPBF than in EBM. This is most probably because of a higher oxide content in the reused powder in case of the LPBF. These oxide layers are formed continuously during each layer of the process. When a new powder layer is applied and molten, the oxide layer is broken and dragged up to the next layer. This accumulation of oxides can also separate and form large, irregular inclusions in the bulk material and consequently create a LOFD [4],[33]. These strings of oxides are the best indicators of where the porosity was located - an example is shown in figure 4.8. The EDX pictures of the oxide can be seen in figure 4.9 - this analysis shows that the oxide layer contains mainly aluminium-rich oxide with traces of titanium. This is expected because Al and Ti are the strongest oxide formers.

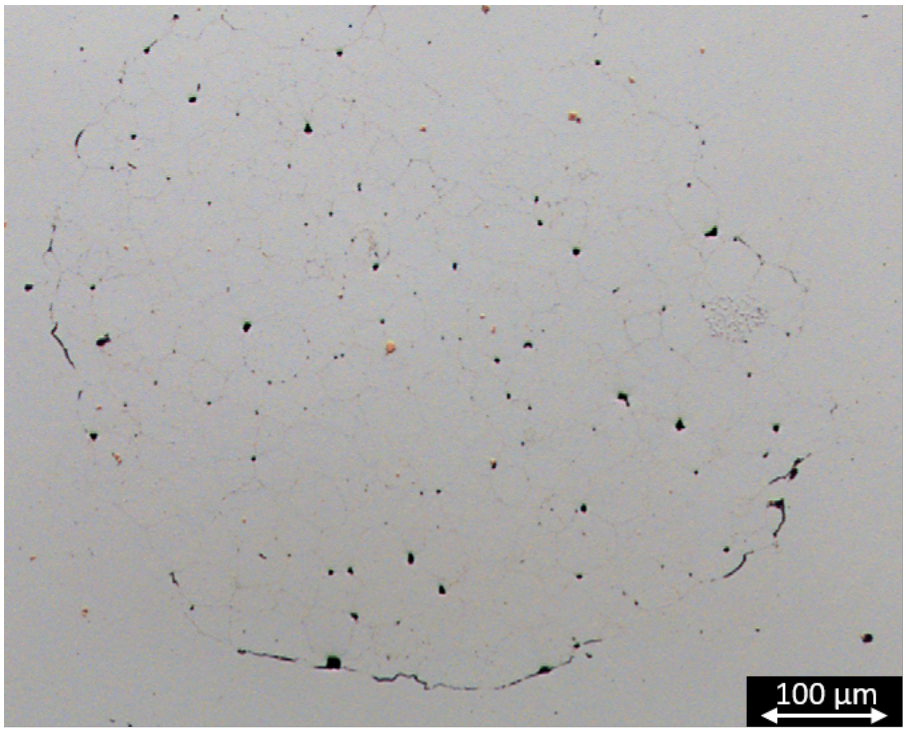

Figure 4.8: LPBF, HIP 3, pressurised ageing, 10 mm cylinder, showing the oxide film accumulated in the bottom of the sphere

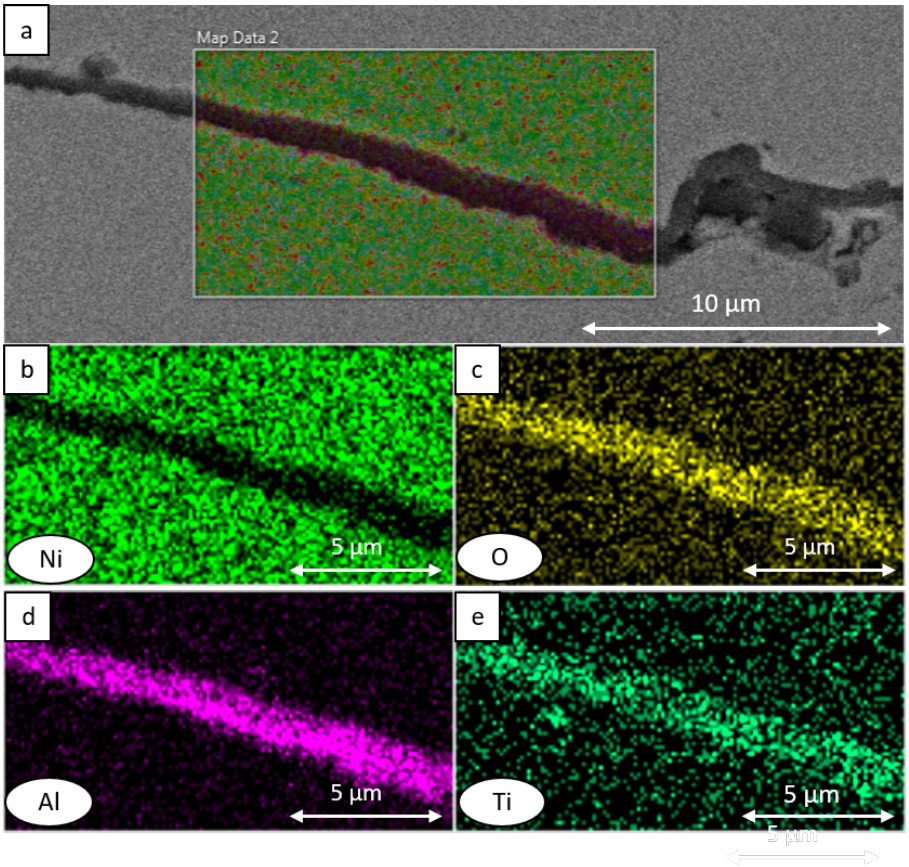

Figure 4.9: LPBF, HIP 4, standard ageing, 5 mm cylinder. a, View of oxide accumulation in the bottom of the sphere and also the mapped area. b-e, elements of the oxide.

The porosities that are not fully closed in the LPBF samples are located either at the previous particle boundaries (PPB) or at the inner rim of the sphere. There is no visible difference between the 5 mm and 10 mm cylinders in terms of the amount of porosity closure in both LPBF and EBM. The most probable reason for this porosity is that the argon cannot diffuse through the material. Therefore, the distance between the porosity and the outer surface of the sample will not affect the result.

4.5.1 HIP 1

The HIP 1 cycle was performed for 5 minutes at 1120°C and 150 MPa. This cycle was not sufficient to fully close the porosity in either LPBF or EBM. The powder did though start to sinter together, as can be seen in figure 4.10 - the spherical shape is still visible and the porosities around the sphere can be seen.

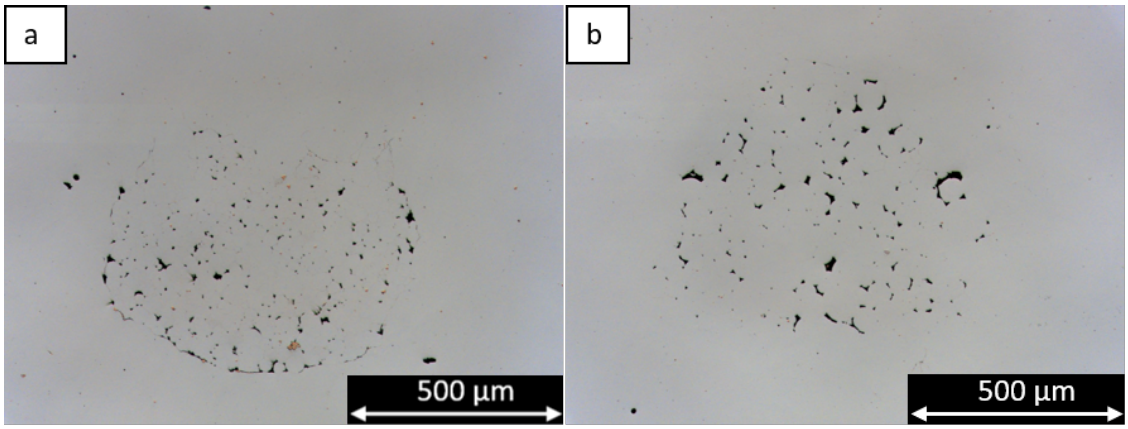

Figure 4.10: a, LPBF, HIP 1, Aged inside HIP, void in 5 mm cylinder. b, EBM, HIP 1, Aged inside HIP, void in 5 mm cylinder. Building direction is upwards.

4.5.2 HIP 2

The HIP 2 cycle was done for 60 minutes at 1120°C. It is difficult to see where the porosity was located in the EBM samples. This indicates that the HIP 2 cycle is enough to fully close the porosities in EBM built samples. At high enough resolution (around 500x) it is possible to see the PPB in the EBM samples. The fact that they are still visible at this high resolution, indicates small amounts of oxides on the prior powder particles. In the LPBF samples there were still small pores left between the prior powder particles - see figure 4.11.

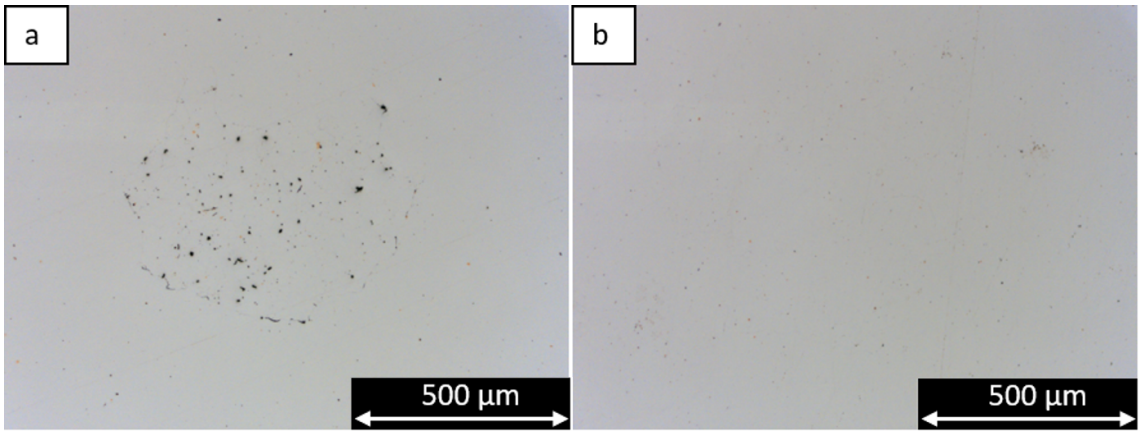

Figure 4.11: a, LPBF, HIP2, as HIPped, void in 5 mm cylinder. b, EBM, HIP2, as HIPped, void in 5 mm cylinder. Building direction is upwards.

4.5.3 HIP 3

The HIP 3 cycle was done at 1120°C for 120 minutes. There is a small difference between HIP 2 and HIP 3 in terms of porosity closure. Porosities in the EBM samples are closed (as seen in HIP 2), whilst samples from LPBF still showed small porosities between powder particles. This is shown in figure 4.12.

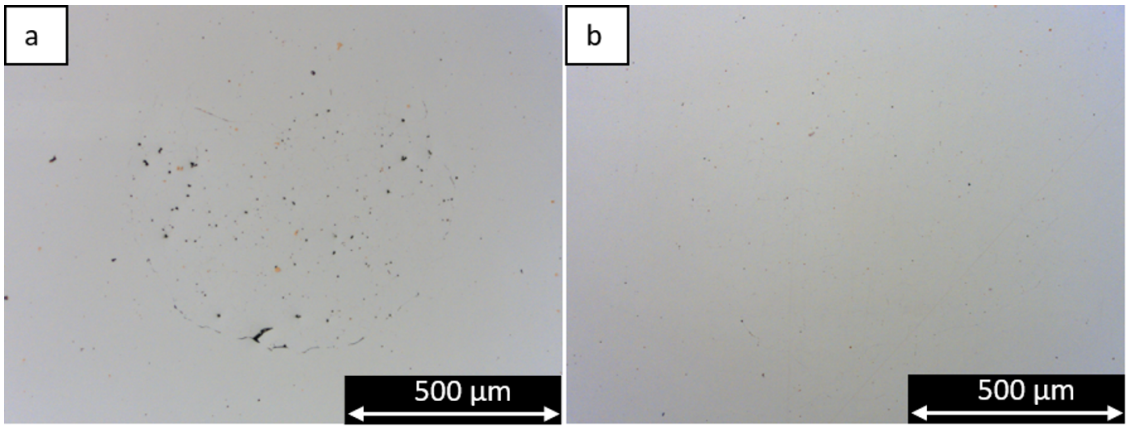

Figure 4.12: a, LPBF, HIP3, as HIPped, void in 5 mm cylinder. b, EBM, HIP3, as HIPped, void in 5 mm cylinder. Building direction is upward.

4.5.4 HIP 4

After 6 hours and 1120°C there was still porosity visible in the sphere in the samples manufactured by LPBF. The EBM sample porosity was closed, as shown in figure 4.13. This proves that the samples manufactured by LPBF contain trapped argon gas from the building chamber atmosphere during printing. It is also proven that even though the time is far longer than normal, there is still porosity in the sphere. It can therefore be concluded that argon cannot diffuse through IN718 even after long HIPing times. It should be emphasised that the porosities are small in comparison with the starting condition before HIP.

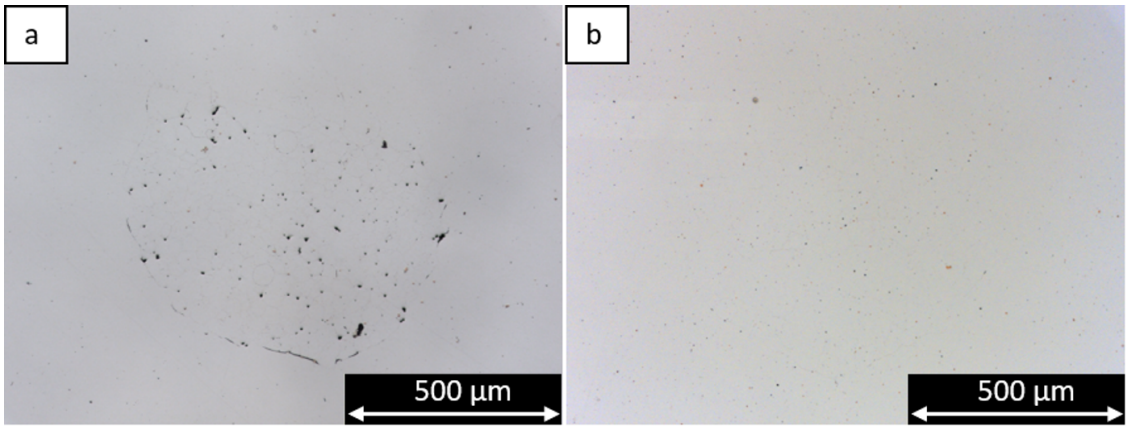

Figure 4.13: a, LPBF, HIP 4, pressurised ageing, void in 10 mm cylinder. b, EBM, HIP 4, aged with pressure, void in 5 mm cylinder. Building direction is upwards.

4.5.5 HIP 5

At a slightly higher temperature of 1180°C holding time of 4 hours, the porosity was still not closed in the LPBF samples. That proves that even at a slightly higher temperature (1180°C instead of 1120°C), the gas porosities cannot be fully closed. From HIP cycles 4 and 5 for LPBF samples, it can be concluded that argon-filled porosities cannot be fully removed during HIPing at temperatures that do not create excessive grain growth. However, these results do not prove that argon cannot be HIPed away at higher temperatures closer to the T_m. Higher HIPing temperatures are though not recommended because of the excessive grain growth that will occur.

The porosity in the EBM samples was fully closed after HIP cycle 5, see figure 4.14. Excessive grain growth could be observed in EBM samples HIPped at this temperature, which correlates with [29]. The increased temperature is therefore not needed, because porosity closure is already achieved during the HIP 2 cycle (at 1120°C for 60 min). The effect of the regrowth of the porosities is not taken in consideration. The regrowth effect should be considered during impact testing.

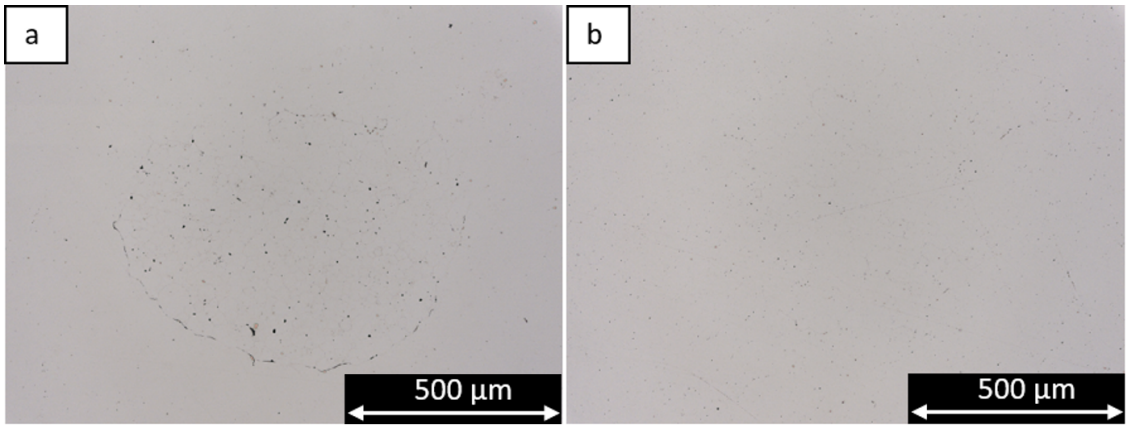

Figure 4.14: a, LPBF, HIP 5, as HIPped, void in 10 mm cylinder. b, EBM, HIP 5, as HIPped, void in 5 mm cylinder. Building direction is upwards.

4.6 Void regrowth

After HIPing, the material needs to be precipitation hardened to obtain its strength. According to the AMS 5664 standard, the material should undergo a solution treatment before ageing - this is at a temperature of 1065°C. If there is still gas left in the material, it could regrow to a new equilibrium size at the ageing pressure [3]. The new equilibrium size would still be much smaller than before the HIP cycle, but now the porosity has a higher internal pressure. Porosity measurements based on one section of the designed sphere indicates a regrowth of 15-190% in the LPBF samples in relation to the porosity after HIP, this can be seen in figure 4.15. It is important to emphasise that each result is only from one compared cut section of each of the spheres. The transparent bar results are from both after HIP and after pressurised ageing - this is because not all cut sections were in the centre of the sphere and the sample closest to the centre was chosen. However, a clear trend can be observed. This should though be investigated further with volumetric measurements by CT scanning in order to statistically verify the magnitude of regrowth. An example of the regrowth can be seen in figure 4.16.

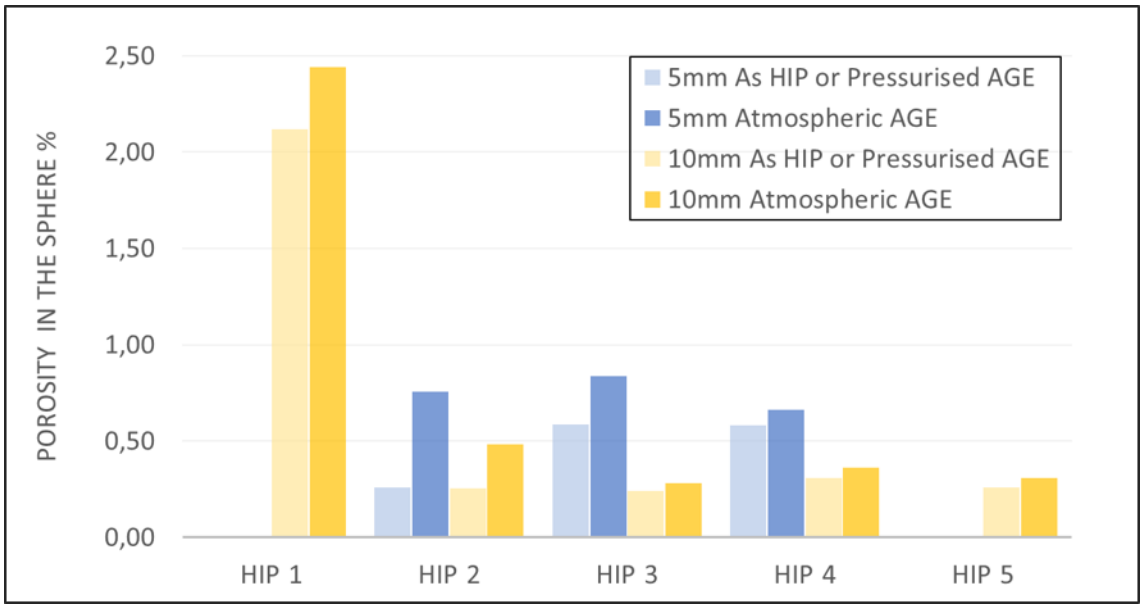

Figure 4.15: LPBF porosity regrowth during subsequent heat treatment after HIP. The transparent bars show the porosity content after HIP or after pressurised ageing. The solid bars shows the porosity content after atmospheric ageing.

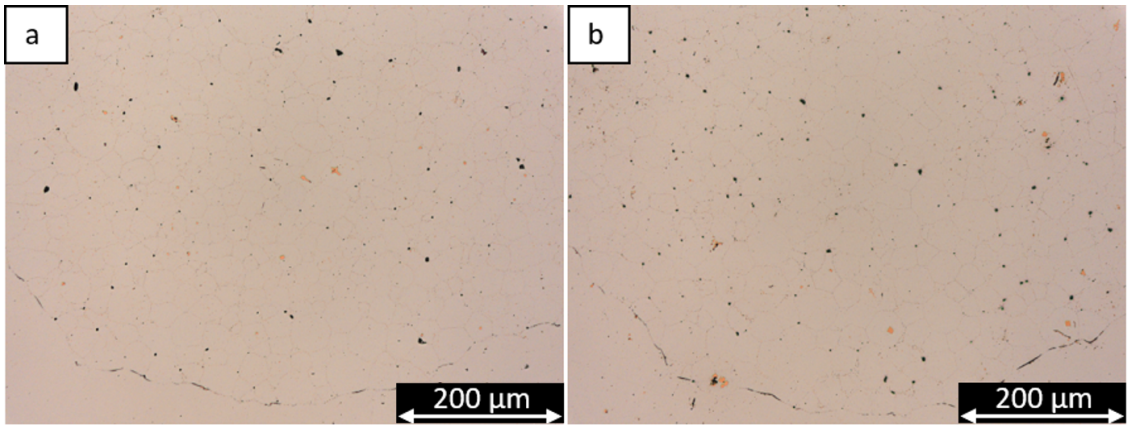

Figure 4.16: LPBF, HIP 5, sphere in 10 mm cylinders. Building direction is upwards. a, pressurised ageing. b, atmospheric ageing.

These results correlate with previous studies into the regrowth of argon porosity during subsequent heat treatment [3]. It is, however, not entirely comparable, because in these investigations CT scans were performed on the same sample prior to HIP and after HIP, as well as after each of the subsequent heat treatments. CT scanning is shown to be an excellent tool as it can be used to follow a specific porosity through the different heat and pressure treatments. CT scanning can also be used to verify

porosity regrowth in the samples; however, in this thesis the porosities are small - often below 5 µm. The resolution for CT scanning are shown to recognise pores at the equivalent size of 5,2 µm in article [3], [36]. This was for small machined

cubic samples of 1,75 x 1,75 x 1,75 mm. The cylinders in this thesis are as small as 5 mm and it would be possible to machine them to decrease the diameter to as little as 1,75 mm. However, if the sphere is 1 mm in diameter, it would only leave 0,375 mm of solid defected-free material around the sphere. This could be difficult to reproduce, especially if there are high accumulation of oxide around the sphere.

4.7 Microstructure inside sphere

The designed sphere can be seen as a large LOFD. It contains powder that is sintered together during the HIPing cycles. After all the HIP cycles in both manufacturing techniques, it is still possible to see the PPBs. This is because the PPB are decorated with small oxides and nitrides. These oxides and nitrides are from the outer surface of reused powder particles and accumulate progressively [4]. During the ageing cycles, δ-precipitates form at the grain boundaries and the inner rim of the sphere. There is no visible intragranular δ-precipitation in the samples that are aged under pressure.

EBM samples contain lower amounts of oxides and fewer twin boundaries. This implies that, if the sphere is seen as LOFD, these EBM samples should have a higher fatigue life as compared to the LPBF built samples [16],[34],[35]. [32] show that it is not possible for LOFD defects with oxides inside to be healed through HIP and that these defects are detrimental for fatigue life. LOFD often contain oxides which cannot be removed with HIP because of the high solution temperature of oxides. It was shown that the amount of accumulated oxides in reused powder continuously increases the more times it is reused, which has detrimental effects on the mechanical properties [4],[32].

4.7.1 LPBF

The unmolten powder particles inside the sphere are sintered together during the HIP. This process creates high stresses and big deformations on the material. As seen inside the sphere, many of these powder particles have developed annealing twins [16] - see figure 4.19. These twins have been shown to be detrimental for the fatigue life of printed parts [35].

Carbides, that was not the MC type primary carbide, was seen to be inside the sphere or in contact with the sphere. Details about these particles and their EDX point measurements are shown in figures 4.17 and 4.18 - the chemical composition of these carbides is given in table 4.2. Figure 4.18 shows a large titanium nitride marked as spectrum 20. It is suspected that these could be $M_{23}C_6$ carbides, but no supporting literature could be found for AM IN718. They are however seen in wrought material especially around high deformation zones [22]. This corresponds well to the high strains in the HIPed powder particles. The measured $M_{23}C_6$ in [22] have a higher Mo and Nb content than the carbides measured in 4.2. These complex carbides and the primary metal can be replaced by many other metals - in this case,

Ni and Fe. On the other hand, the high Si content could indicate that it is rather a M_6C carbide.

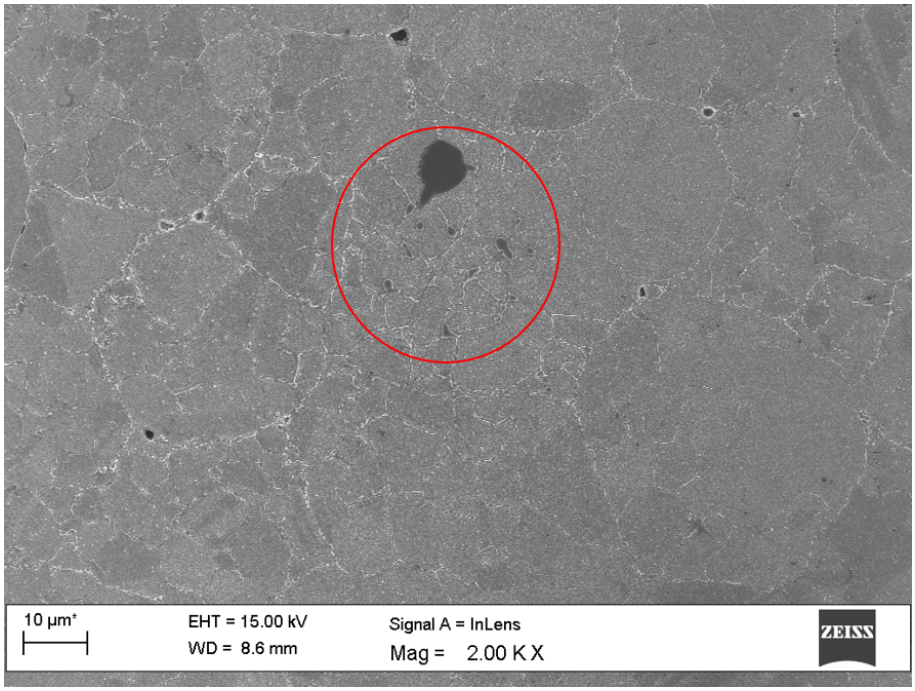

Figure 4.17: LPBF, HIP 3, pressurised ageing, inside the sphere. Showing a large nitride and also some smaller carbides. The red circle showing where figure 4.18 is located.

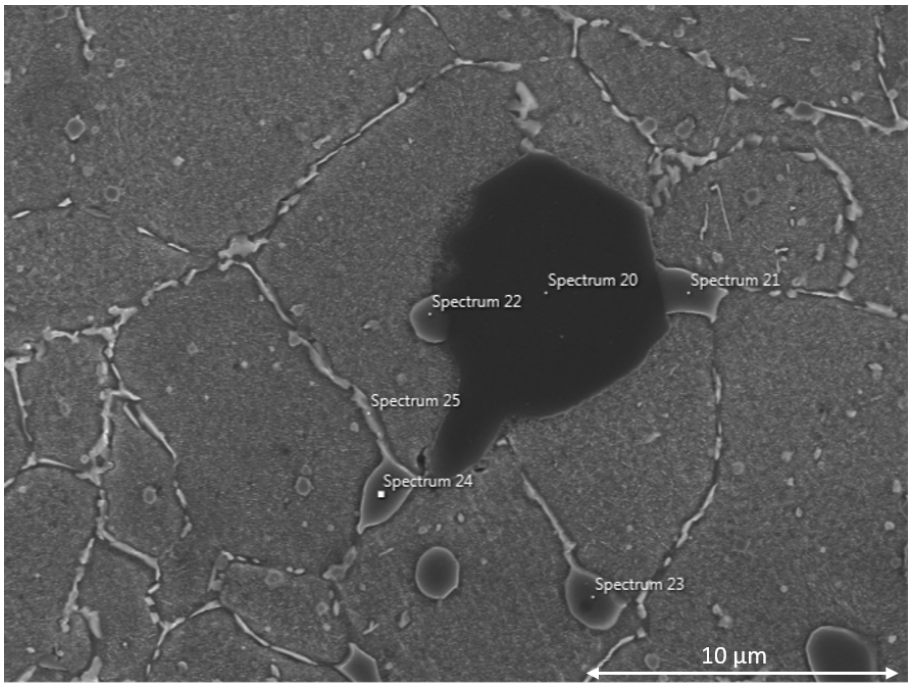

Figure 4.18: LPBF, HIP3, pressurised ageing. Points where EDX point measurements are performed. Results can be seen in table 4.2

.

Table 4.2: EDX point measurement of points in figure 4.18

Material	Ni	Nb	Fe	Mo	Cr	Si	C	Ti	N
Point 21-24, Wt%	34,2	25,7	11,2	11	10,4	3,4	3,4	0,8	-
$M_{23}C_6$ [22], Wt%	3,8	39,5	3,6	34,2	18,8	-	-	-	-
Point 20, Wt%	-	10,2	-	-	3,2	-	-	68,4	19,3

The main strengthening precipitation, γ'', shows no difference in size or distribution both inside and around the sphere. This indicates that the adhered powder particles in the LOFD would have the same strength as the surrounding material after HIP and ageing.

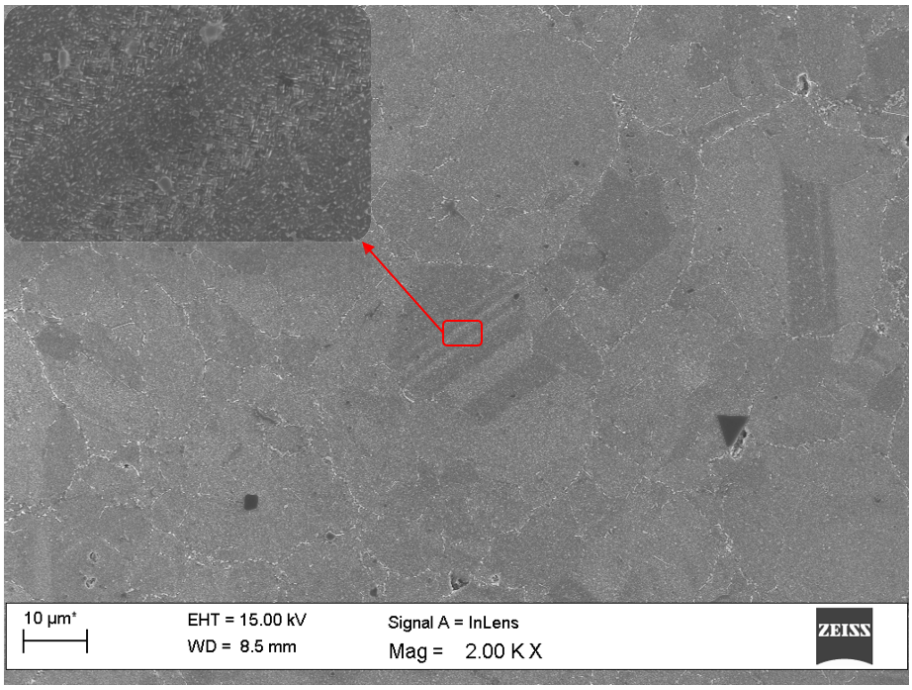

Figure 4.19: LPBF, HIP 3, pressurised ageing, 5 mm cylinder. Inside the sphere there is many twins in the previous powder particle. The picture shows a higher magnification of a grain with many twin boundaries.

4.7.2 EBM

As can be seen in figure 4.20, the grain growth from the HIP 5 cycle (1180°C for 240 minutes) is obvious. It is interesting to note that many carbides have nucleated at some places on the rim of the sphere - this can be seen in figure 4.21. These carbides could be a complex carbide type $M_{23}C_6$. However, it is not possible to conclude this for certain. This amount of Nb carbides are undesirable because it depletes the area from Nb, which is the γ'' component.

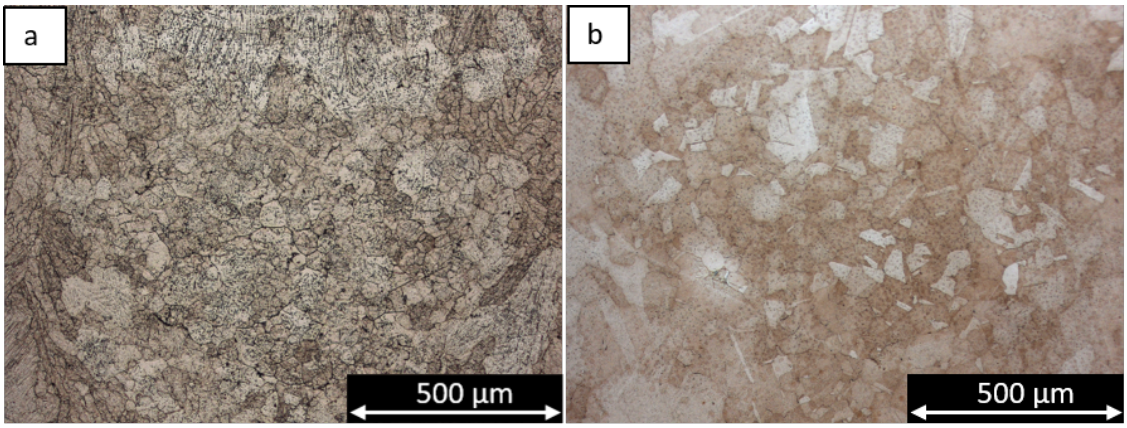

Figure 4.20: a, EBM, HIP 3, 1120°C, 120min, pressurised ageing, showing no abnormal grain growth. b, EBM HIP 5, 1180°C, 240min, pressurised ageing, showing abnormal grain growth.

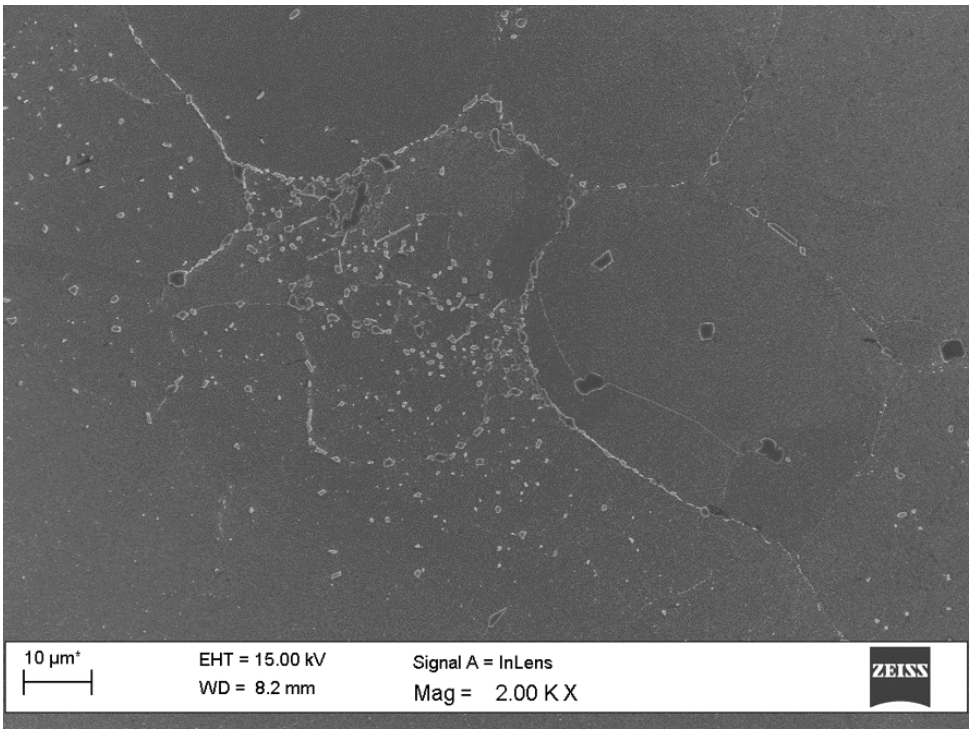

Figure 4.21: EBM HIP 5, 1180°C, 240min, pressurised ageing. Image is taken at the outer rim of the sphere. In the top right half of the image prior particle boundaries are visible inside the sphere and bottom left are outside the sphere. Image shows possible $M_{23}C_6$ carbides formed during long HIPing time at high temperature in the melted area outside the sphere.

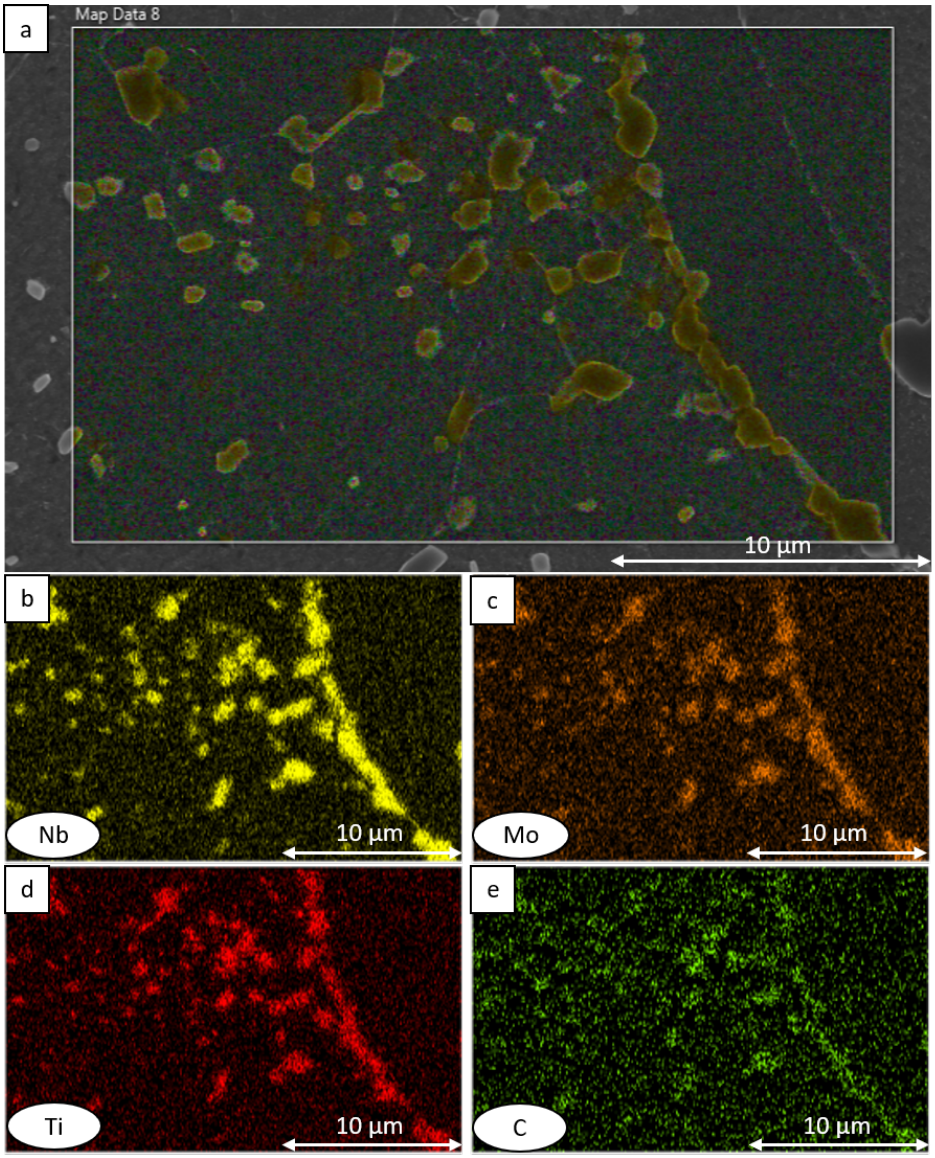

Figure 4.22: EBM HIP 5, 1180°C, 240min, pressurised ageing. The outer rim of the sphere, mapped area of carbides from figure 4.21. a, mapped area. b-e, composition of the carbides.

4.8 Future work

The amount of the porosity inside the different samples should be examined using CT scanning. It could be of particular interest to follow an individual sample through the different cycles - because all the samples are different, the amount of entrapped gas in the sphere could vary.

The different HIP and ageing cycles need to be evaluated to determine their effects on the mechanical properties of the samples. The impact toughness bars produced as part of this thesis work should be tested as part of this evaluation.

The evaluation of porosity closure in LBPF could be repeated with virgin powder to determine if the oxide accumulation affects the mechanical properties and extent of porosity closure in AM IN718 samples.

5
Conclusions

Two different series of cylinders with a 1 mm powder-filled sphere were produced using both laser powder bed fusion (LPBF) and electron beam melting (EBM). These cylinders underwent five different hot isostatic pressing (HIP) cycle variations and two different ageing cycles. The different ageing cycles were performed either inside the HIP furnace under pressure or at atmospheric pressure.
In the LPBF produced samples it was not possible to fully close the porosities in the sphere even after 360 minutes at 1120°C and a pressure of 150 MPa. In EBM, however, 60 minutes at 1120°C under a pressure of 150 MPa was enough to fully close the porosities. From this it can be concluded that the LPBF porosities that are filled with argon cannot be fully closed by HIP. In addition, it has to be emphasised that recycled powder was used in case of LPBF that can be partly responsible for rather poor pore closure in case of LPBF.

An increase in pressure during ageing of LPBF samples showed a reduction in visible porosity regrowth after heat treatment. It has to be emphasised that the regrowth is small but clear especially compared to the size before HIP. EBM samples were fully closed after HIP and did not show any porosity regrowth during atmospheric ageing.

The powder-filled sphere is a highly effective way to follow a lack of fusion defect (LOFD) through different HIPing processes. Although the sphere is larger than any typical defect found in AM, this allows for the examination of the effects of HIPing on a LOFD.

- Large porosities filled with argon in LPBF samples cannot be completely removed by HIPing although the remaining size is much smaller than the initial size.
- Argon filled porosities in LPBF samples regrow during subsequent heat treatment after HIP. However this regrowth is very small compared to the initial size.
- Representing a LOFD with a powder-filled sphere has proven to be efficient method to study the effects of different HIP and heat treatment cycles on the behaviour of LOFD in additively manufactured components.

Bibliography

[1] William E. Frazier, "Metal Additive Manufacturing: A Review," *Journal of Materials Engineering and Performance*, vol. 23, no. 6, pp. 1917-1928, June 2014. Available: https://doi.org/10.1007/s11665-014-0958-z

[2] Gokuldoss Prashanth Konda, Kolla Sri, Eckert Jürgen, "Additive Manufacturing Processes: Selective Laser Melting, Electron Beam Melting and Binder Jetting—Selection Guidelines", *Materials*, vol. 10, no. 6, June 2017. Available: https://doi.org/10.3390/ma10060672

[3] S. Tammas-Williams, P.J. Withers, I. Todd, P.B. Prangnell, "Porosity regrowth during heat treatment of hot isostatically pressed additively manufactured titanium components", *Scripta Materialia*, vol. 22, pp. 72-76, 2014. Available: https://doi.org/10.1016/j.scriptamat.2016.05.002

[4] H. Gruber, "Electron Beam Melting of Alloy 718, Powder Recycling and its Effect on Defect Formation", LiC. Thesis, Dept of Industrial and Materials Science., Chalmers Uni., Gothenburg Sweden, 2019. Available: https://research.chalmers.se/en/publication/?id=507691

[5] Mujian Xia, Dongdong Gu, Guanqun Yu, Donghua Dai, Hongyu Chen, Qimin Shi, "Porosity evolution and its thermodynamic mechanism of randomly packed powder-bed during selective laser melting of Inconel 718 alloy" *International Journal of Machine Tools and Manufacture*, vol. 116, pp. 96-106, May 2017. Available: https://doi.org/10.1016/j.ijmachtools.2017.01.005

[6] Ross Cunningham, Andrea Nicolas, John Madsen, Eric Fodran, Elias Anagnostou, Michael D. Sangid, Anthony D. Rollett, "Analyzing the effects of powder and post-processing on porosity and properties of electron beam melted Ti-6Al-4V", *Materials Research Letters*, vol. 5, no. 7, pp. 516-525, 2017. Available: https://doi.org/10.1080/21663831.2017.1340911

[7] Tahira Raza, Joel Andersson, Lars-Erik Svensson, "Microstructure of selective laser melted alloy 718 in as-manufactured and post heat treated condition", *Procedia Manufacturing*, vol. 25, pp. 50-458, 2018. Available: https://doi.org/10.1016/j.promfg.2018.06.100

[8] Atkinson H.V, Davies S, "Fundamental Aspects of Hot Isostatic Pressing: An Overview", *Metallurgical and Materials Transactions A*, vol. 31, no. 12, pp. 2981-3000, December 2000. Available: https://doi.org/10.1007/s11661-000-0078-2

[9] Shih-Hsien Chang, Shih-Chin Lee, Tzu-Piao Tang, Hsin-Hung Ho, "Influences of Soaking Time in Hot Isostatic Pressing on Strength of Inconel 718 Superalloy", *MATERIALS TRANSACTIONS*, vol. 47, no. 2, pp. 426-432, 2006. Available: https://doi.org/10.2320/matertrans.47.426

[10] Watson, JE 2011, *Superalloys*, Production, Properties and Applications, Nova Science Publishers, Incorporated, New York. Available from: ProQuest Ebook Central.

[11] Wang Xiaoqing, Gong X, Chou K, "Review on powder-bed laser additive manufacturing of Inconel 718 parts", *Proceedings of the Institution of Mechanical Engineers, Part B: Journal of Engineering Manufacture*, vol. 231, no. 11, pp. 1890-1903, January 2016. Available: https://doi.org/10.1177/0954405415619883

[12] Manuela Galati, Luca Iuliano, "A literature review of powder-based electron beam melting focusing on numerical simulations", *Additive Manufacturing*, vol. 19, pp. 1-20, January 2018. Available: https://doi.org/10.1016/j.addma.2017.11.001

[13] Jingchao Jiang, Xun Xu, Jonathan Stringer, "Support Structures for Additive Manufacturing: A Review", *Manufacturing and materials processing*, vol. 2, no. 4, art number. 64, September 2018. Available: https://doi.org/10.3390/jmmp2040064

[14] Haijun Gong, Khalid Rafi, Hengfeng Gu, Thomas Starr, Brent Stucker, "Analysis of defect generation in Ti–6Al–4V parts made using powder bed fusion additive manufacturing processes", *Additive Manufacturing*, vol. 1-4, pp. 87-98, June 2017. Available: https://doi.org/10.1016/j.addma.2014.08.002

[15] W. J. Sames, F. A. List, S. Pannala, R. R. Dehoff, S. S. Babu, "The metallurgy and processing science of metal additive manufacturing", *International Materials Reviews*, vol. 61, no. 5, March 2016. Avaliable: https://doi.org/10.1080/09506608.2015.11166499

[16] G.Appa Rao, Mahendra Kumar, M. Srinivas, D.S. Sarma, "Effect of standard heat treatment on the microstructure and mechanical properties of hot isostatically pressed superalloy inconel718", *Materials Science and Engineering: A*, vol. 355, no. 1, pp. 114-125, August 2003. Available: https://doi.org/10.1016/S0921-5093(03)00079-0

[17] Keisuke Sano, Naoko Oono, Shigeharu Ukai, Shigenari Hayashi, Toshihiko Inoue, Shinichiro Yamashita, Tsunemitsu Yoshitake "γ'' precipitate in Fe–Ni base alloy", *Journal of Nuclear Materials*, vol. 442, no. 1, pp. 389-393, November 2013. Available: https://doi.org/10.1016/j.jnucmat.2013.07.037

[18] Matthew J. Donachie, Stephen J. Donachie, *Superalloys: A Technical Guide, 2nd Edition*, publisher ASM International, pp, 28-36, 2002. ISBN: 9781615030644.

[19] V.A. Popovich, E.V. Borisov, A.A. Popovich, V.Sh. Sufiiarov, D.V. Masaylo, L. Alzina, "Impact of heat treatment on mechanical behaviour of Inconel 718 processed with tailored microstructure by selective laser melting", *Materials & Design*, vol. 131, pp. 12-22, October 2017. Available: https://doi.org/10.1016/j.matdes.2017.05.065

[20] A. Mitchell, "PRIMARY CARBIDES IN ALLOY 718", 7th symposioum of superalloys and derivatives, TMS(The mineral, metals and material society) 2010. Available: https://www.tms.org/superalloys/10.7449/2010/Superalloys_2010_161_167.pdf

[21] Oradei-Basile. Armida, Radavich. John F, "A current TTT diagram for wrought alloy 718", *Superalloys*, Vol. 718, no. 625, pp. 325-335, 1991.

[22] Aghajani. Ali, Tewes. Jürgen, Parsa. Alireza Basir, Hoffmann. Thorsten, Kostka. Alexander, Kloewer. Jutta, "Identification of Mo-Rich M23C6 Carbides in Alloy 718", *Metallurgical and Materials Transactions A*, Vol. 47, no. 9, pp. 4382-4392, September 2016. Avaliable:`https://doi.org/10.1007/s11661-016-3593-5`

[23] A. Strondla, R. Fischerb, G. Frommeyera, A. Schneider, "Investigations of MX and γ'/γ'' precipitates in the nickel-based superalloy 718 produced by electron beam melting", *Materials Science and Engineering: A* vol. 480, no. 1-2, pp. 138-147, May 2008. Available: `https://doi.org/10.1016/j.msea.2007.07.012`

[24] J. E. Matz and T. W. Eagar, "Carbide formation in alloy 718 during electron-beam solid freeform fabrication", *Metallurgical and Materials Transactions A*, vol. 33, no. 8, pp. 2559–2567, 2002. Available: `https://doi.org/10.1007/s11661-002-0376-y`

[25] John D. Roehling, William L. Smith, Tien T. Roehling, Bey Vrancken, Gabriel M. Guss, Joseph T. McKeown, Michael R. Hill, Manyalibo J. Matthews, "Reducing residual stress by selective large-area diode surface heating during laser powder bed fusion additive manufacturing", *Additive Manufacturing*, vol. 28, pp. 228-235, August 2019. Avaliable: `https://doi.org/10.1016/j.addma.2019.05.009`

[26] *Nickel Alloy, Corrosion and Heat Resistant, Bars, Forgings, and Rings, 52.5Ni - 19Cr - 3.0Mo - 5.1Cb - 0.90Ti - 0.50Al - 18Fe, Consumable Electrode or Vacuum Induction Melted, 1950 °F (1066 °C) Solution Heat Treated, Precipitation Hardenable*, AMS standard 5664, 1965.

[27] Joseph R. Davis, *Metals Handbook* 10th ed, USA, ASM International, 1990.

[28] M. I. Moulding, Kroeger Jens, Marion Frédéric, "Leading the way with plasma atomised Ti spherical powders for MIM", *PIM International* vol. 5, no. 4, pp. 55–57, December 2011.

[29] Sneha Goel, "Post-treatment of Alloy 718 produced by electron beam melting", Lic. Thesis, Dept Engineering Science, Trollhättan Sweden, 2019. Avaliable: `http://www.diva-portal.se/smash/get/diva2:1289341/FULLTEXT01.pdf`

[30] Mostafa Ahmad, Picazo Rubio Ignacio, Brailovski Vladimir, Jahazi Mohammad, Medraj Mamoun, "Structure, Texture and Phases in 3D Printed IN718 Alloy Subjected to Homogenization and HIP Treatments", *Metals*, vol. 7, no. 6, art number. 196, 2017. Available: `https://doi.org/10.3390/met7060196`

[31] Sneha Goel, Jonas Olsson, Magnus Ahlfors, Uta Klement, Shrikant Joshi, "The Effect of Location and Post-treatment on the Microstructure of EBM-Built Alloy 718",*Journal of Materials Engineering and Performance*, vol. 28, no. 2, pp. 673-680, February 2019. Available: `https://doi.org/10.1007/s11665-018-3712-0`

[32] Balachandramurthi Arun Ramanathan, Moverare Johan, Mahade Satyapal, Pederson Robert "Additive Manufacturing of Alloy 718 via Electron Beam Melting: Effect of Post-Treatment on the Microstructure and the Mechanical Properties" *Materials*, vol. 12, no. 1, pp. 19-25, December 2018. Available: `https://doi.org/10.3390/ma12010068`

[33] Xiangfang Xu,Jialuo Ding, Supriyo Ganguly, Chenglei Diao, Stewart Williams, "Oxide accumulation effects on wire + arc layer-by-layer additive manufacture process", *Journal of Materials Processing Technology*, vol. 252, no. 1-2, pp. 739-750, May 2018. Available: https://doi.org/10.1016/j.jmatprotec.2017.10.030

[34] Sean Gribbin, Jonathan Bicknell, Luke Jorgensen, Igor Tsukrov, Marko Knezevic, "Low cycle fatigue behavior of direct metal laser sintered Inconel alloy 718", *International Journal of Fatigue*, vol. 93, pp. 156-167, December 2016. Available: https://doi.org/10.1016/j.ijfatigue.2016.08.019

[35] Clayton A. Stein, Albert Cerrone, Tugce Ozturk, Sukbin Lee, Peter Kenesei, Harris Tucker, Reeju Pokharel, Jonathan Lind, Christopher Hefferan, Robert M. Suter, Anthony R. Ingraffea, Anthony D. Rollett, "Fatigue crack initiation, slip localization and twin boundaries in a nickel-based superalloy", *Current Opinion in Solid State and Materials Science*, vol. 18, no. 4 pp. 244-252, August 2014. Available: https://doi.org/10.1016/j.cossms.2014.06.001

[36] S. Tammas-Williams, H. Zhao, F. Léonard, F. Derguti, I. Todd, P.B. Prangnell, "Titanium, Additive Manufacture, Selective Electron Beam Melting, Pores, X-ray Computed Tomography (XCT)", *Materials Characterization*, vol. 102, no. 6, pp. 47-61, April 2015. Avliable: https://doi.org/10.1016/j.matchar.2015.02.008

A

Appendix 1

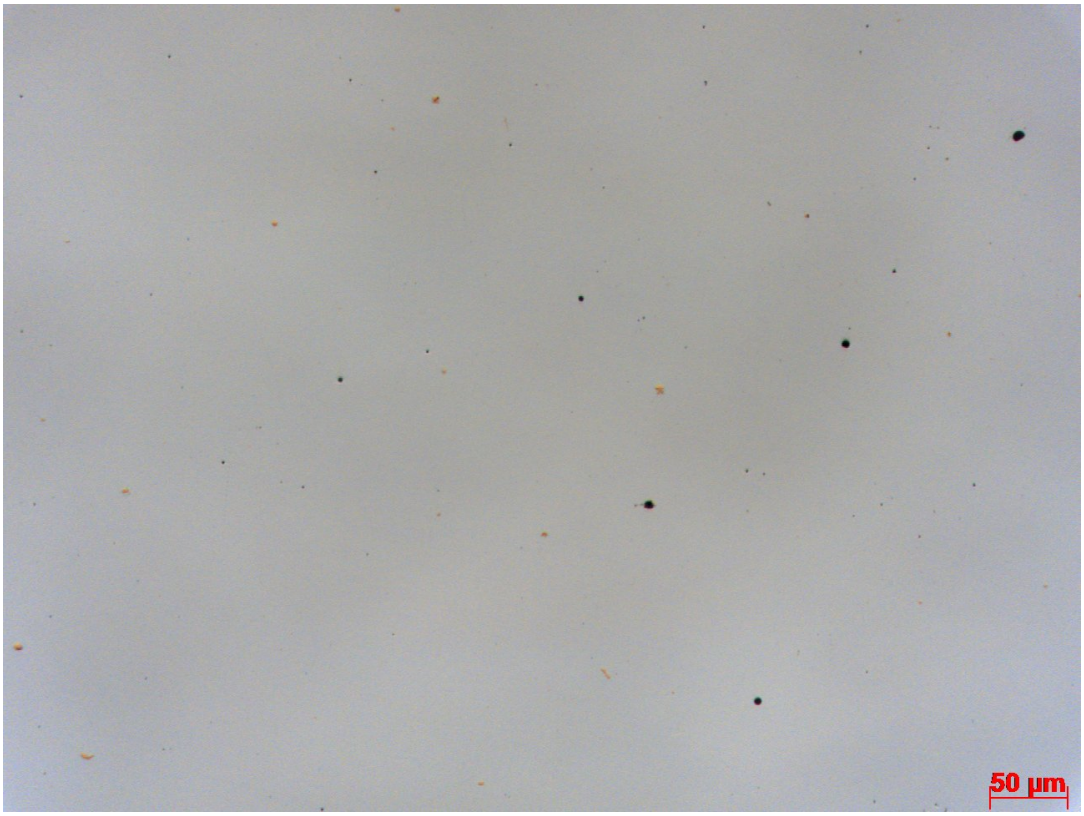

Figure A.1: Picture for porosity measurement. Sample As-built DMLS 10mm cylinder picture 4/15.

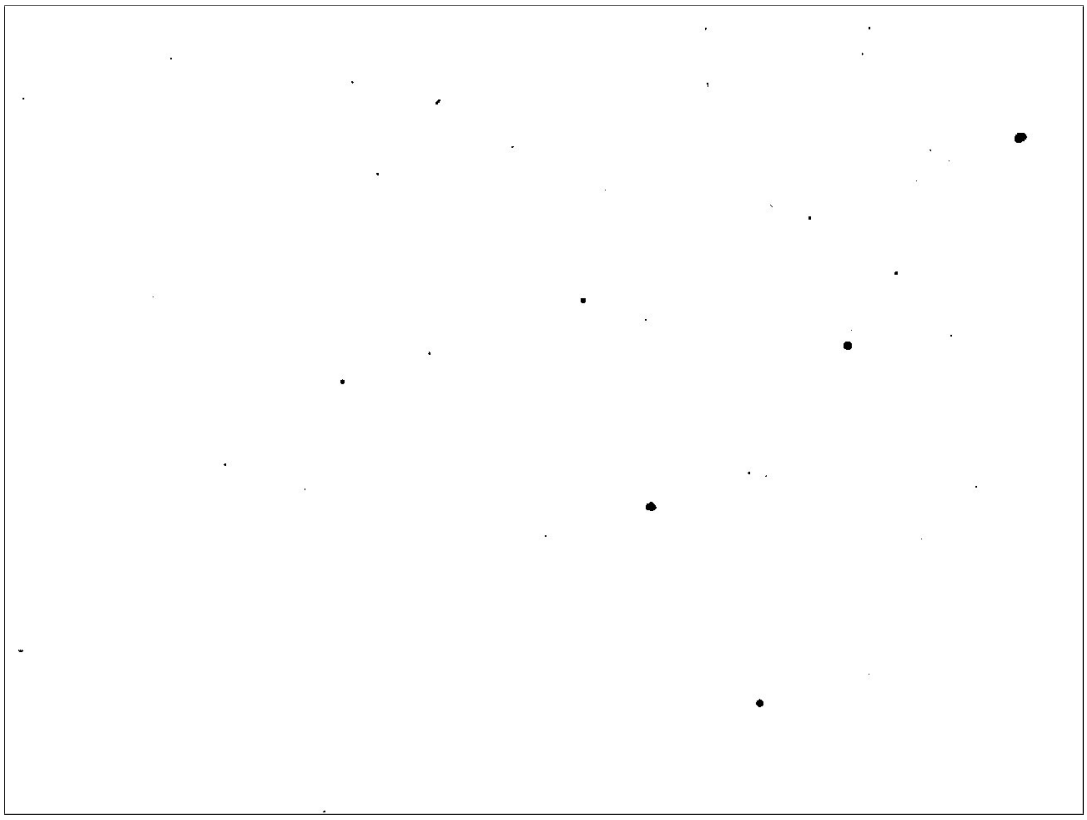

Figure A.2: Scale bar removed and threshold adjusted to only show porosity and not Nitrides. Amount of pores measured, 0,05% in this picture